JOURNAL OF VIROLOGY, Oct. 2009, p. 9786–9802 Vol. 83, No. 19
0022-538X/09/$08.00+0 doi:10.1128/JVI.00704-09

Disruption of LANA in Rhesus Rhadinovirus Generates a Highly Lytic Recombinant Virus▽†

Kwun Wah Wen,[1,2,3] Dirk P. Dittmer,[1,2,3]* and Blossom Damania[1,2,3]*

Lineberger Comprehensive Cancer Center, University of North Carolina at Chapel Hill, Chapel Hill, North Carolina 27599[1]; Department of Microbiology and Immunology, University of North Carolina at Chapel Hill, Chapel Hill, North Carolina 27599[2]; and Center for AIDS Research, University of North Carolina at Chapel Hill, Chapel Hill, North Carolina 27599[3]

Received 5 April 2009/Accepted 2 July 2009

Rhesus monkey rhadinovirus (RRV) is a gammaherpesvirus that is closely related to human Kaposi's sarcoma-associated herpesvirus (KSHV/HHV-8). RRV is the closest relative to KSHV that has a fully sequenced genome and serves as an in vitro and an in vivo model system for KSHV. The latency-associated nuclear antigen (LANA) protein of both KSHV and RRV plays key roles in the establishment and maintenance of these herpesviruses. We have constructed a RRV recombinant virus (RRVΔLANA/GFP) in which the RRV LANA open reading frame has been disrupted with a green fluorescent protein (GFP) expression cassette generated by homologous recombination. The integrity of the recombinant virus was confirmed by diagnostic PCR, restriction digestion, Southern blot analysis, and whole-genome sequencing. We compared the single-step and multistep replication kinetics of RRVΔLANA/GFP, RRV-GFP, wild-type (WT) RRV H26-95, and a revertant virus using traditional plaque assays, as well as real-time quantitative PCR-based genome quantification assays. The RRVΔLANA/GFP recombinant virus exhibited significantly higher lytic replicative properties compared to RRV-GFP, WT RRV, or the revertant virus. This was observed upon de novo infection and in the absence of chemical inducers such as phorbol esters. In addition, by using a quantitative real-time PCR-based viral array, we are the first to report differences in global viral gene expression between WT and recombinant viruses. The RRVΔLANA/GFP virus displayed increased lytic gene transcription at all time points postinfection compared to RRV-GFP. Moreover, we also examined several cellular genes that are known to be repressed by KSHV LANA and report that these genes are derepressed during de novo lytic infection with the RRVΔLANA/GFP virus compared to RRV-GFP. Finally, we also demonstrate that the RRVΔLANA/GFP virus fails to establish latency in B cells, as measured by the loss of GFP-positive cells and intracellular viral genomes.

Kaposi's sarcoma-associated herpesvirus (KSHV), or human herpesvirus 8, is a member of the *Gammaherpesviridae* subfamily. This virus has been implicated as the etiological agent of Kaposi's sarcoma (9) and lymphoproliferative diseases of B-cell origin, namely, primary effusion lymphoma (PEL) (8) and the plasmablastic variant of multicentric Castleman's disease (28, 78).

A detailed understanding of KSHV replication and pathogenesis is important for understanding the biology of the diseases that are associated with this virus. However, in vivo studies of KSHV are limited due to the inability of KSHV to persistently infect mice or rhesus macaques (23, 68). Furthermore, difficulties are encountered when trying to study KSHV replication in vitro (67). Although several groups have described the use of endothelial cells to investigate de novo KSHV replication (19, 44, 67, 72), the virus replicates lytically only for a limited number of rounds before entering latency in these cells. Hence, virus titers of KSHV are quite low in endothelial cells, and plaques were rarely observed. Another system to generate lytic virus involves the treatment of KSHV-infected PEL cell lines with 12-*O*-tetradecanoyl-phorbol-13-acetate (TPA) or *n*-butyrate (56, 70). The problem here is that only a small subset (25 to 30%) of latently infected PEL lymphocytes can be artificially reactivated with TPA (56, 70). Thus, the heterogeneous nature of the lytically and latently infected cell populations hampers the dissection of the function of individual viral genes in the context of the whole virus.

We have used rhesus monkey rhadinovirus (RRV) to model KSHV pathogenesis in rhesus fibroblasts (RhF) (59). RRV was identified by Desrosiers et al. in 1997 at the New England Primate Research Center as a gammaherpesvirus of rhesus macaques (*Macaca mulatta*) (15). This isolate was designated H26-95. In addition, Wong et al. at the Oregon Regional Primate Research Center isolated a different strain of RRV (designated 17577) from simian immunodeficiency virus (SIV)-infected macaques (88). Sequence analysis revealed that the two RRV isolates are homologous to each other, although not identical. Importantly, both genomes exhibit colinearity with the KSHV genome (1, 76), and all RRV genes have homologues in KSHV (1, 76). Wong et al. showed that in SIV-infected macaques, RRV induced B-cell hyperplasia resembling KSHV multicentric Castleman's disease (88), as well as non-Hodgkin's lymphoma (60). Mansfield et al. reported that RRV also caused an arteriopathy in SIV-infected macaques (54).

* Corresponding author. Mailing address: Lineberger Comprehensive Cancer Center, CB#7295, University of North Carolina, Chapel Hill, NC 27599. Phone: (919) 843-6011. Fax: (919) 966-9673. E-mail for B. Damania: damania@med.unc.edu. E-mail for D. P. Dittmer: ddittmer@med.unc.edu.

† Supplemental material for this article may be found at http://jvi.asm.org/.

▽ Published ahead of print on 8 July 2009.

RRV presents several advantages for studying lytic replication. First, the RRV life cycle can be modeled in vivo, in rhesus macaques. Second, RhF support 100% lytic replication of RRV and allows for the production of high titers of virus (~10^6 PFU/ml) (58). Our group has demonstrated that the transcription program of RRV is similar to that of KSHV (17, 25). Several laboratories have used the RRV model to study viral gene products, including the viral interleukin-6 homologue (37), Rta/Orf50, R8/RAP, R8.1 (17, 50), R1 (13, 14), R15 (46, 63), RRV Orf4 (55), and the RRV-encoded microRNAs (74). We previously reported the kinetics of gene expression with regard to immediate-early, early, and late genes during RRV lytic infection and have reported that they are similar to those seen during KSHV reactivation (17, 25). We also generated a RRV-green fluorescent protein (GFP) recombinant virus and devised plaque assays and real-time quantitative PCR (QPCR) assays for the determination of virus titers (18). This validates the experimental methods used here.

The KSHV latency-associated nuclear antigen (K-LANA) maintains latency by tethering the circularized viral episome to the mitotic host chromosomes, which allows the viral genome to cosegregate with the host genome to daughter cells during cell division (5–7, 11, 12, 33, 38, 39, 41, 42, 65, 69, 80, 87, 89, 90). We have previously reported the identification and characterization of RRV LANA (R-LANA) (16). R-LANA shows homology to K-LANA except for the central variable-length internal acidic repeat domain, which is absent in R-LANA. The N- and C-terminal ends of R-LANA show high degree of sequence similarity to K-LANA, containing the same arrangement of chromosome-binding domain, nuclear localization signal, and proline/serine-rich and glutamine-rich regions. Similar to K-LANA, R-LANA exhibited a speckled nuclear localization (16). We have previously reported that R-LANA can bind the RRV viral genome and may tether the RRV genome to the host chromosome in a fashion similar to that observed with K-LANA (16).

Genetically, both K-LANA and R-LANA are encoded by open reading frame (ORF) 73 (Orf73) of their respective viruses. K-LANA is found in the tricistronic latency-associated cassette, which also includes Orf71/vFLIP and Orf72/vCyclin (22, 73, 82). Differential splicing of the tricistronic cassette results in a 1.7-kb bicistronic transcript containing Orf72 and Orf71. Thus, the expression of KSHV Orf71, Orf72, and Orf73 is coordinately driven by the common LANA promoter. Within the bicistronic transcript, there exists an internal ribosome entry site in Orf72 for protein translation of Orf71. Although expressed at low levels, monocistronic Orf71 transcript was also detected during KSHV latency, and this transcript was upregulated during lytic reactivation, suggesting that there might be a cryptic promoter for Orf71 expression during the lytic cycle (31). In RRV, similarly arranged tricistronic (LANA, vCyclin, and vFLIP) and bicistronic (vCyclin and vFLIP) transcripts have been previously described by our group (17). In KSHV, LANA has also been shown to transactivate its own promoter (35, 36, 62, 79). In addition, as a possible mechanism to ensure K-LANA expression during the lytic cycle, Rta (replication transcription activator) was described to positively regulate K-LANA gene expression by recruiting RBP-Jκ to the LANA promoter (45). K-LANA, on the other hand, has been shown to inhibit Rta transactivation of downstream viral promoters by various mechanisms (reviewed in reference 84).

Our lab has previously demonstrated that R-LANA inhibits RRV Rta transactivation of lytic promoters (16). In order to examine the role of R-LANA protein in the RRV life cycle, we have disrupted the expression of R-LANA in the viral genome by using homologous recombination. We describe here the construction of a RRVΔLANA/GFP knockout virus and compare the replication kinetics of RRVΔLANA/GFP, RRV-GFP, and wild-type (WT) RRV H26-95 at three different multiplicities of infection (MOIs; 0.1, 0.5, and 5) using traditional plaque assays, as well as real-time PCR-based genome quantification assays. We have also constructed an RRV revertant virus (RRV_{REV}) and find that it behaves similarly to WT RRV.

Previously, LANA knockout viruses have been published for KSHV and murine gammaherpesvirus 68 (MHV68) (26, 27, 47, 57). The KSHV LANA deletion virus showed higher viral replication than did WT KSHV in vitro. The MHV68 LANA-null virus showed no difference in replication in vitro at a high MOI and a lower amount of replication in vitro than did WT MHV68 at very low MOIs (27, 47, 57). These experiments yielded important insights but also raised new questions. RRV is the closest relative to KSHV that has a de novo infection system. We constructed a RRVΔLANA/GFP knockout virus and have examined RRV LANA's contribution to the lytic and latent cycle. We found that RRVΔLANA/GFP exhibits enhanced lytic replication similar to the KSHV LANA deletion virus. In addition, this higher lytic replication is seen upon de novo infection and in the absence of chemical inducers such as TPA. Furthermore, we are the first to use a real-time QPCR-based RRV array to transcriptionally profile genomewide viral gene expression during de novo infection with RRVΔLANA/GFP and RRV-GFP viruses. We also analyzed several cellular genes that were previously reported to be repressed by KSHV LANA alone and found that they were derepressed in RRVΔLANA/GFP-infected cells compared to RRV-GFP-infected cells. This suggests that R-LANA modulates transcription of these genes during lytic infection and in the context of the whole virus.

MATERIALS AND METHODS

Cell culture. Immortalized rhesus macaque skin fibroblasts (i.e., RhF) with puromycin resistance were described previously (17). Cells were maintained at 37°C and 5% CO_2 in Dulbecco modified Eagle medium-H (DMEM-H) with Glutamax supplemented with 10% fetal bovine serum (FBS), penicillin, and streptomycin. BJAB cells, a human B-cell line that is KSHV negative and Epstein-Barr virus (EBV) negative were maintained in RPMI 1640 medium supplemented with 10% fetal bovine serum, penicillin, and streptomycin.

Construction of the recombinant RRVΔLANA/GFP virus and the revertant RRV_{REV} virus. The RRV isolate H26-95 (15) and RRV-GFP (18) were previously described. To construct RRVΔLANA/GFP, a 3,051-bp sequence of RRV H26-95 spanning nucleotides 117207 to 121414 containing R-LANA and flanking sequences was PCR amplified with the primers 5′-CGCCGCGAATTCCGGTC AATGGAGAGCATCAGGTG-3′ and 5′-CGCCGCAAGCTTCGCGCGCTCA CATAGACCTATAC-3′. This amplicon was subsequently cloned into pSp72 (Promega) at EcoRI and HindIII restriction sites to create pSp72-R-LANA-flank (also called R-LANA-flank plasmid). Site-directed mutagenesis was performed to create a SacI site at nucleotide position 40 of the R-LANA ORF with the primers 5′-CAGGAACTTCGCAACCCGAGCTCCGATACTATGCCGG AAC-3′ and 5′-GTTCCGGCATAGTATCGGAGCTCGGGTTGCGAAGTTC CTG-3′. The resulting plasmid was designated pSp72-R-LANA-flank-new SacI. The enhanced GFP (EGFP) expression cassette driven by the cytomegalovirus (CMV) immediate-early (IE) promoter with the simian virus 40 polyadenylation

TABLE 1. Cellular genes that are activated (derepressed) in RRVΔLANA/GFP-infected RhF compared to RRV-GFP-infected RhF

Gene	Accession no.[a]	dC_T			ddC_T		Fold derepression[b]	Reference
		Mock	RRV-GFP	RRVΔLANA	RRV-GFP-Mock	RRVΔLANA-Mock		
NCOA3	XM_001101475	5.473	1.128	2.619	–4.345	–2.854	2.810	2
CREBL1	XR_014255	6.574	4.835	6.065	–1.739	–0.509	2.344	2
CCAAT-box binding transcription factor	XM_001084362	8.765	5.425	7.406	–3.34	–1.359	3.946	2
CCND2	XR_012297	6.253	3.497	5.034	–2.755	–1.219	2.902	77
FKHL1/FOXG1B	XM_001106922	13.406	9.521	12.981	–3.885	–0.425	11.005	77
Actin (control)	NM_001033084	–2.304	–2.796	–2.573	–0.492	–0.269	1.167	

[a] That is, under *Macaca mulatta*.
[b] Calculated as: (2^{ddCT} RRVΔLANA)/(2^{ddCT} RRV-GFP).

signal was PCR amplified from a pEGFP-N1 (Clontech) plasmid in which the multiple cloning site was removed by digesting with BamHI and BglII and religating the ends together. The EGFP-N1 cassette primers used were 5′-CAAAAAGAGCTCGTAATCAATTACGGGGTCAT-3′ and 5′-CAAAAAGAGCTCACCACAACTAGAATGCAGTG-3′. The resulting SacI-tagged CMV-GFP-pA amplicon was ligated into pSP72-R-LANA-flank-new SacI to form pSp72ΔLANA/GFP (also called R-LANA-flank+GFP plasmid). This plasmid was linearized by EcoRI digestion and then transfected into RhF by using the Amaxa Nucleofection system as described by the manufacturer. At 48 h post-nucleofection, RhF were infected with RRV H26-95 virus at a low MOI. A single GFP-positive virus was isolated and purified by limiting dilution and plaque assay five times. To generate a revertant virus, RhF were nucleofected with EcoRI-linearized pSp72-R-LANA-flank plasmid and subsequently infected with RRVΔLANA/GFP at a low MOI. Clear, GFP-negative plaques were isolated, and the revertant virus was further separated from RRVΔLANA/GFP by three rounds of plaque purification. This revertant virus was designated RRV_{REV}.

Viral DNA of RRV-H26-95, RRVΔLANA/GFP, or RRV_{REV} was used as a template for PCR analysis with the R-LANA flanking primers 5′-CGCCGCGAATTCCGGTCAATGGAGAGCATCAGGTG-3′ and 5′-CGCCGCAAGCTTCGCGCGCTCACATAGACCTATAC-3′ and the R-LANA primers 5′-GAGTTGGAATTC TTAGTGCTGAATTGGCAG-3′ and 5′-CGGCAATCTAGATTAGTGCTGAATTGGCAGTCCTCTGTCCATGCGCACTATGC-3′.

Southern hybridization. Virus was harvested from virus-infected RhF by centrifugation at 17,000 rpm for 3 h. The virus pellet was resuspended in phosphate-buffered saline, treated with Sarkosyl, and subsequently treated with proteinase K at 60°C for 1 h. Viral DNA was extracted by the phenol-chloroform method. For Southern blot analysis, 1 μg of the viral DNA was digested with NheI for hybridization with the RRV LANA probe or digested with SacI for hybridization with the GFP probe. Digestion fragments of viral genomic DNA were subjected to electrophoresis through 1% low-melting-point agarose (NuSieve) and transferred overnight to a nylon membrane (Hybond N+) by capillary action. After UV cross-linking, the membranes were prehybridized in QuikHyb solution at 65°C for 15 min. Probes were generated from a 330-bp RRV LANA fragment restriction digested by KpnI and FspI (R-LANA ORF nucleotides 985 to 1315) and a 154-bp GFP fragment (nucleotides 362 to 515 from the ATG start codon of EGFP-N1 plasmid) derived from PCR by the random prime method using ^{32}P-labeled dCTP (Roche). Probes were denatured at 95°C for 3 min and added to QuikHyb Prehybe solution (Stratagene). Hybridization was carried out for 1 h at 65°C. The probe solution was removed, and the membranes were washed twice for 15 min with 2× SSC (1× SSC is 0.15 M NaCl plus 0.015 M sodium citrate)–0.1% sodium dodecyl sulfate at room temperature and once for 30 min at 60°C with 0.1× SSC–0.1% sodium dodecyl sulfate. Membranes were exposed overnight on an X-ray film.

Illumina/Solexa sequencing. Supernatant of RRV-infected RhF was filtered, concentrated by ultracentrifugation, and loaded on a Sepharose CL-4B column (Sigma) to isolate RRV virions. RRV genomic DNA was released by Sarkosyl and proteinase K (Qiagen) treatment, and purified by phenol-chloroform extraction. The viral DNA was further purified by using a Wizard SV genomic DNA purification system (Promega) according to the manufacturer's instructions. A portion (4 μg) of RRVΔLANA DNA was submitted to UNC-CH Genome Analysis Facility and sequenced by using an Illumina/Solexa 1G genome analyzer with the Illumina DNA sample preparation kit (FC-102-1001), a standard cluster generation kit (FC-103-1001), and an 18-cyle Illumina sequencing kit (FC-104-1001). This sample was sheared to 200 to 300 bp by using a Bioruptor. Library preparation then followed standard Illumina protocols for a GA2 sequencer (Illumina, San Diego, CA). The Illumina GA2 sequencer was run with 36 cycles using the standard flow cell. Raw Illumina GA2 sequence image data were phased and filtered for quality using the default GERALD parameters for unaligned reads (analysis, none; used bases, 35). Sequence reads were aligned to the RRV genome using the emboss function fuzznuc (71) and CLC Genomics Workbench V2.0.4 (CLC Bio, Inc.) under Mac OS X, v10.5.5. Further analysis was conducted by using R (GNU general public license [http://www.gnu.org/licenses/licenses.html#GPL]). For the junction search, raw sequence data were first converted into a BLAST database using formatdb, and then the predicted junction fragments 5′-ATGTCCCCTGCAGGAACTTCGCAACCCGAGCT_CGTAATCAATTACGGGGTCATTAGTTCAT and 5′-TTTTTTCACTGCATTCTAGTTGTGGTGAGCT_CCGATACTATGCCGGAACGATGTTGCCG (underscores mark the junctions) were searched against the Illumina read database.

Real-time QPCR for viral load and cellular gene expression analysis. For each sample, 10 μg of salmon sperm carrier DNA was added to 200 μl of clarified supernatant from infected cells and processed through a DNeasy kit (Qiagen, Valencia, CA) according to the manufacturer's protocol. To quantify viral DNA, SYBR green real-time PCR in a 384-well format was performed using an ABI Prism 7900 sequence detection system (Applied Biosystems, Inc., Foster City, CA). To generate a standard curve for cycle thresholds (C_Ts) versus genomic copy numbers, the pcDNA3-RRVOrf50 plasmid was serially diluted to known concentrations in the range of 10^1 to 10^6 plasmid molecules/μl. Each PCR mixture (15 μl) contained 4 μl of viral or standard DNA, 1 μl of the Orf50 primer set (final working concentration, 3.33 μM), 7.5 μl of SYBR green 2× PCR mix (Applied Biosystems), and 2.5 μl of DNase- and RNase-free water (Sigma) in a total volume of 15 μl. Primers for amplification of an 81-bp amplicon internal to the Orf50 sequence were 5′-GTGGAAAGCGGTGTCACAGA-3′ and 5′-TGCGGCGGCCAAAAT-3′. The PCR conditions were as follows: 95°C for 15 min, followed by 95°C for 15 s and 60°C for 1 min repeated for 40 cycles. Similar reactions were assembled to assess cellular gene expression. The sequences for real-time PCR primers for the specific cellular genes shown in Table 1, including β-actin (housekeeping control), are provided in Table 2.

Plaque assays. RhF monolayers in 12-well plates were achieved by plating 2×10^5 cells per well 2 days before starting the assay. Tenfold dilutions of virus-infected cell supernatants were made in DMEM-H supplemented with 2% fetal bovine serum (FBS). Each sample dilution was performed in triplicate. A total of 200 μl of each dilution was placed in each well of 12-well dishes, followed by incubation at 37°C, with redistribution of the inoculum every 15 min. Importantly, for all infections, we incubated the virus with the cells for exactly 2 h, after which the inoculum was aspirated, and an overlay of methylcellulose was added to each well. The overlay medium consisted of (per well): 1 ml of 2× DMEM, 1 ml of 1.5% methyl-cellulose (Sigma catalog no. M0512), and 40 μl of FBS (2%). The cells were then incubated for 7 days at 37°C and 5% CO_2. The overlay medium was then aspirated, and the cells were stained with 0.8% crystal violet (Sigma catalog no. C3886) in a 50% ethanol staining solution for 1 h. Plaques were counted under ×10 magnification.

RRV real-time PCR genome array. The RRV quantitative real-time reverse transcription-PCR genome array was previously described (25). Samples were prepared for the viral array as follows. Virus was used to infect RhF at an MOI of 0.5. The infected RhF were centrifuged and snap-frozen at −80°C at 12, 24, 48, 72, 96, 120, and 144 h postinfection. RNA from RRV-infected RhF was isolated using RNAzol (Tel-Test, Inc.) as previously described (24, 25). Poly(A) mRNA was prepared using dT-beads (Qiagen) and reverse transcribed by using Superscript II reverse transcriptase (Life Technologies) according to the manu-

TABLE 2. Real-time QPCR primers for rhesus cellular genes

Gene	Primer sequence (5′–3′)	
	Forward	Reverse
NCOA3	GGGGATGGTGAGCTGTGACT	TGACATCCAAAATGGTCAGCA
CREBL1	TGAGGTGGGGGTGTTC	GAGCTCTATATTCCGAAAAGG
CCAAT-box binding transcription factor	TTTCAAGTCCTTTCACCCCAG	GCAAGGCTGTTTTTTACCCC
CCND2	ATTGGCTATGATGGTGACAT	CTCTTAAAAGGCAGCTGACTA
FKHL1/FOXG1B	AAGAAAGTTGTTTCAGTTGGC	TTCAATTGAATGGGCAGT
β-Actin	CCTTCCATCGTCCACCGCAAATGCTTCTAGGC	GTCAAGAAAGGGTGTAACGCAACTAAGTCACA

facturer's recommendations. Then, 500 ng of RNA was reverse transcribed by using an ABI cDNA archive kit and random hexanucleotide primers (Applied Biosystems, Inc.). The reaction mixture was sequentially incubated at 42°C for 45 min, 52°C for 30 min, and 70°C for 10 min. The reverse transcription reaction was quenched by heating to 95°C for 5 min and then subjected to 0.5 U of RNase H (Invitrogen) treatment at 37°C for an additional 30 min. Afterward, the cDNA pool was diluted 25-fold with diethyl pyrocarbonate-treated, distilled H_2O and stored at −80°C. For quantitative real-time PCR, 2.5 μl of primer mix was combined with 7.5 μl of SYBR green 2× PCR mix (Applied Biosystems) and 5 μl of cDNA and subjected to real-time QPCR on an MJR Opticon2 cycler using standard cycling conditions.

RRV infection of BJAB cells. A total of 2×10^5 BJAB cells were spinoculated in flat-bottom 12-well plates with 1.5 ml of diluted viral stock in complete RPMI medium in the presence of 4 μg of Polybrene/ml as previously described (85). The cells were washed once with complete RPMI medium and then allowed to grow and expand in complete RPMI medium.

RESULTS

Generation of a RRVΔLANA/GFP recombinant virus. Our lab has previously published the generation of an RRV recombinant virus expressing GFP (RRV-GFP) using homologous recombination (18). We used a similar homologous recombination approach to construct a RRVΔLANA/GFP recombinant virus by inserting a GFP expression cassette into the R-LANA ORF to disrupt R-LANA transcription and translation. A 3,051-bp sequence of RRV H26-95 spanning nucleotides 117207 to 121414 containing R-LANA and flanking sequences was PCR amplified and subcloned into the plasmid pSp72 to create pSp72-R-LANA-flank. We then mutagenized a unique SacI restriction site in the R-LANA ORF in the pSp72-R-LANA-flank plasmid at nucleotide 40 of the R-LANA ORF to generate pSp72-R-LANA-flank-new SacI. The GFP expression cassette was subcloned into this SacI site in a direction opposite to the R-LANA ORF to yield the plasmid pSp72ΔLANA/GFP. Next, the pSp72ΔLANA/GFP plasmid was linearized with EcoRI, and RhF were nucleofected with the linearized pSp72ΔLANA/GFP plasmid, followed by RRV infection at a low multiplicity of infection (Fig. 1A). Single GFP-positive viruses were plaque purified for five rounds, and one such isolate, named RRVΔLANA/GFP, was chosen for further study. Using a similar procedure, we subsequently generated a rescue virus by nucleofection of RhF with EcoRI-linearized pSp72-R-LANA-flank plasmid, followed by infection with RRVΔLANA/GFP at a low MOI (Fig. 1B). Clear, GFP-negative plaques were isolated and separated from GFP-positive RRVΔLANA/GFP by plaque purification. One such revertant virus, designated RRV_{REV}, was chosen for further study.

We have confirmed the correct insertion of the GFP cassette into RRVΔLANA/GFP by diagnostic PCR with two different sets of primers targeting full-length R-LANA ORF and its flanking regions, respectively (Fig. 2A, B, and C). Cell pellets of RhF infected with RRVΔLANA/GFP were subjected to total DNA isolation on DNeasy columns (Qiagen). Approximately 500 ng of total DNA per infected sample was subjected to standard PCR. The R-LANA-flank plasmid (also called the pSp72-R-LANA-flank plasmid in Fig. 1B) or parental H26-95 viral DNA was used as the PCR template as a negative control for GFP insertion. The R-LANA-flank+GFP plasmid (also called pSp72ΔLANA/GFP in Fig. 1A) served as the PCR template for the positive control. The R-LANA primers and R-LANA flanking primers amplified from the R-LANA-flank+GFP plasmid template showed the expected fragment sizes of 2,950 and 5,800 bp, respectively (Fig. 2B and C).

The removal of the GFP sequence in rescue virus RRV_{REV} was likewise confirmed by diagnostic PCR (Fig. 2D, E, and F). Total DNA was isolated from RRV_{REV}-infected RhF pellets and subjected to standard PCR. The R-LANA-flank plasmid DNA or H26-95 viral DNA was used as a control to show the expected amplicon sizes of intact R-LANA (Fig. 2). The PCR products of the RRV_{REV} viral DNA show the correct sizes of 1,350 bp for WT R-LANA ORF with the full-length R-LANA primer set (Fig. 2E) and 4,200 bp for WT R-LANA flank sequence with the R-LANA flank primer (Fig. 2F).

To rule out aberrant insertion of the exogenous GFP cassette into the rest of the viral genome, diagnostic Southern blot analysis after restriction digest was performed. We have provided a graphical scheme of the restriction digestion and Southern blotting in Fig. 3A. Virion DNA from WT RRV H26-95, RRVΔLANA/GFP, and RRV_{REV} recombinant viruses grown on RhF was isolated and digested with NheI. The digested DNA fragments were resolved on two separate agarose gels by electrophoresis, and the gels were transferred and cross-linked to nitrocellulose membrane. Southern blots were performed using a radiolabeled probe complementary to either the R-LANA or the GFP sequence (Fig. 3A). The R-LANA-specific probe hybridized to a predicted 2.4-kb fragment in RRVΔLANA/GFP and a predicted 6.5-kb fragment in RRV H26-95 and RRVΔLANA $_{REV}$ digested with NheI (Fig. 3B). The GFP-specific probe used in the Southern blot revealed the expected hybridization fragment size of 5.6 kb for NheI-digested RRVΔLANA/GFP virion DNA (Fig. 3C). As expected, the probe did not hybridize to the WT H26-95 or the rescue virus DNA. A third Southern blot was performed using the GFP probe (Fig. 3D). Since the GFP cassette in RRVΔLANA/GFP was inserted into the virus at a newly cre-

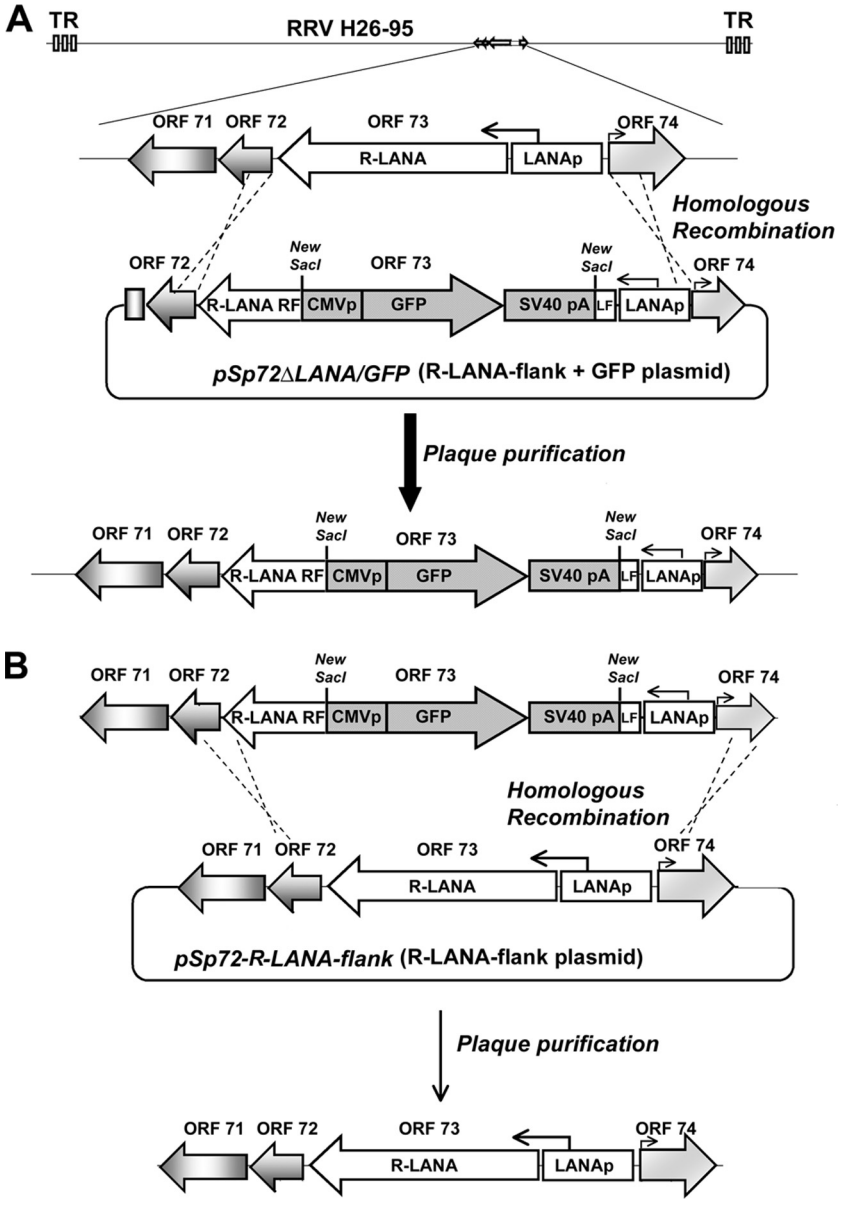

FIG. 1. Schematic representation of the construction of the RRVΔLANA/GFP and RRV_{REV} recombinant viruses. (A) Construction of the RRVΔLANA/GFP virus. An EGFP expression cassette driven by a CMV promoter was inserted into the N terminus of R-LANA (Orf73) to disrupt the R-LANA ORF. This EGFP cassette was cloned into a plasmid containing the coding sequence of R-LANA and flanking ORFs (Orf71 to Orf74). The plasmid (pSp72ΔLANA/GFP) was linearized and transfected into RhF and then subjected to RRV infection at a low MOI. Single GFP-expressing viral plaques were purified for five rounds, and one such isolate, designated RRVΔLANA/GFP, was chosen for further study. (B) Construction of a revertant RRV_{REV} virus. A plasmid containing the coding sequence of R-LANA flanked by Orf71 and Orf74 (pSp72-R-LANA-flank) was linearized and transfected into RhF. Transfected cells were infected with RRVΔLANA/GFP at a low MOI. GFP-negative viral plaques were purified. One such isolate was designated RRV_{REV} and chosen for further study. LF, left flank; RF, right flank.

ated SacI site, restriction digestion with SacI should release a 1.6-kb fragment corresponding to the size of the exogenous GFP sequence from this recombinant virus. In the Southern blot shown in Fig. 3D, this fragment was detected by the GFP probe in SacI-digested virion DNA of RRVΔLANA/GFP but was absent in the SacI-digested H26-95 and RRV_{REV} genomic DNA, as expected. Ethidium bromide-stained gels of SacI single-digested and SacI/EcoRI double-digested RRV H26-95 and RRVΔLANA/GFP viral DNA are shown in Fig. S1 and S2, respectively, in the supplemental material.

Whole-genome sequencing of the RRVΔLANA/GFP recombinant virus. The results from these traditional molecular analyses suggest that the RRVΔLANA/GFP recombinant virus is genetically identical to the WT RRV H26-95 genome, except for the insertion of the GFP expression cassette in the R-LANA ORF. To further ensure complete genetic integrity at the nucleotide level, we performed genomewide sequencing of RRVΔLANA/GFP virus by using the recently developed Illumina/Solexa sequencing technology. It was crucial to obtain highly pure and abundant viral DNA for such a purpose. Ap-

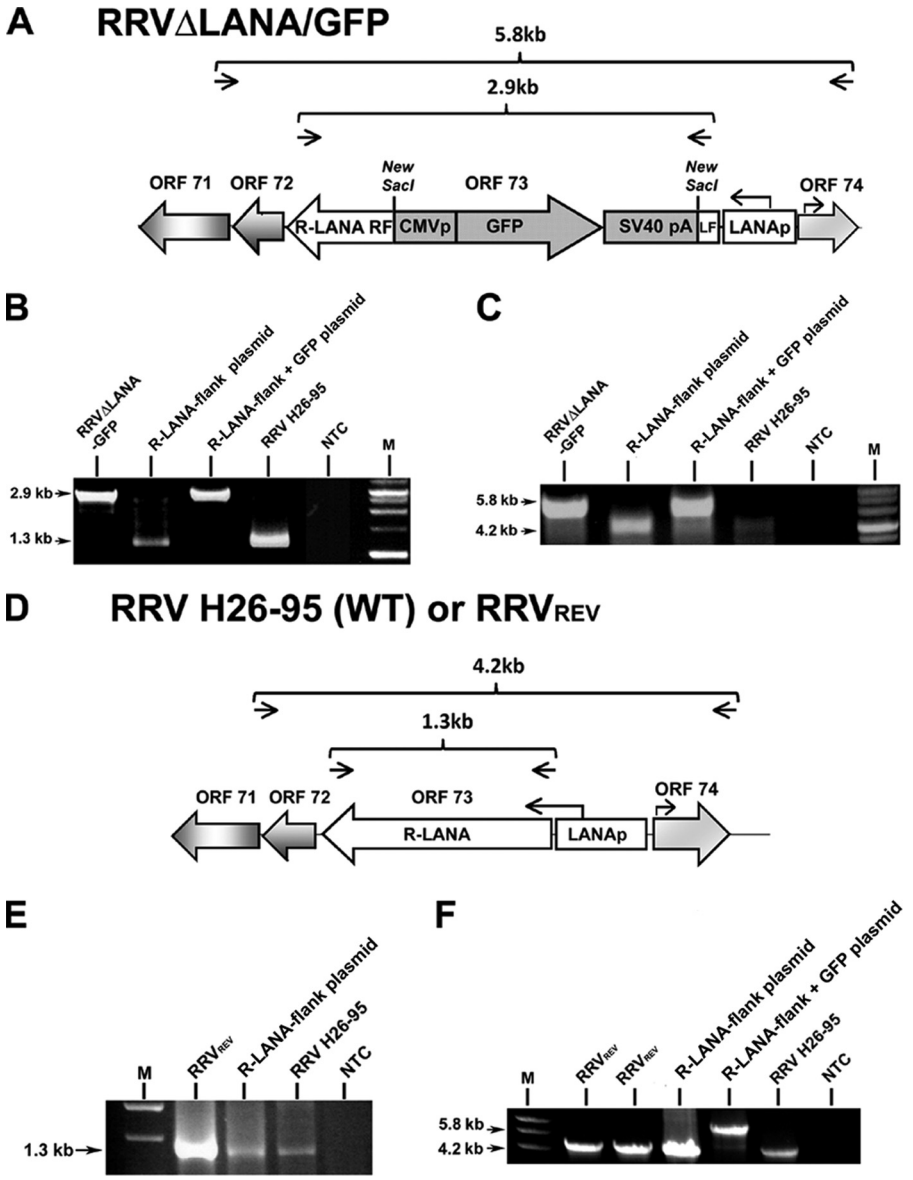

FIG. 2. PCR analysis of recombinant viruses. (A) Schematic representation of PCR diagnosis of RRVΔLANA/GFP virus. Primers (arrows) for either the full-length R-LANA ORF (lower bracket) or the R-LANA flanking ORF (upper bracket). (B) Templates used in the PCRs are labeled on top of each lane. NTC denotes nontemplate control, and M denotes marker. With the R-LANA primer set, the expected size for R-LANA (~1,350 bp) was seen in R-LANA-flank plasmid (i.e., pSp72-R-LANA-flank plasmid in Fig. 1B) and RRV H26-95 viral DNA. The RRVΔLANA/GFP lane and R-LANA-flank+GFP (i.e., pSp72ΔLANA/GFP in Fig. 1A) plasmid lane show the expected size (~2,950 bp) for EGFP cassette (~1,600 bp) insertion. (C) with the R-LANA flanking primer set, an expected size of ~4,200 bp was seen with the R-LANA-flank plasmid and RRV H26-95 viral DNA. The RRVΔLANA/GFP lane and R-LANA-flank+GFP plasmid lane show the expected size (~5,800 bp) for EGFP cassette insertion. (D) A schematic representation of PCR diagnosis of RRV_{REV}. Primers (arrows) for either the full-length R-LANA ORF (lower bracket) or the R-LANA flanking ORF (upper bracket). (E) with the full-length R-LANA primer set, the PCR product of RRV_{REV} shows the correct size for R-LANA ORF, similar to the amplicon size (~1,350 bp) of positive template controls (R-LANA-flank plasmid and RRV H26-95 viral DNA). (F) PCR using the R-LANA flank primer set displays an expected amplicon size (~4,200 bp) for the RRV_{REV} template as indicated by the same amplified fragment size when WT R-LANA-flank plasmid or viral DNA H26-95 was used as the template.

proximately 5×10^8 RhF were subjected to RRVΔLANA/GFP infection, and virus was amplified until a complete cytopathic effect was observed. Cell-free supernatant of RRV-infected RhF was filtered, ultracentrifuged, and subjected to virion purification on a Sepharose column. RRV genomic DNA was released by Sarkosyl and proteinase K treatment and purified by phenol-chloroform extraction. Further purification of genomic DNA was performed by using a Wizard SV genomic DNA purification system (Promega). A portion (4 μg) of RRVΔLANA DNA was submitted to the UNC-CH Genome Analysis Facility. We obtained full coverage of the RRVΔLANA/GFP viral genome when the parental RRV H25-95 (AF210726) excluding the 3′ terminal repeat was used as the reference sequence. We used stringent alignment pa-

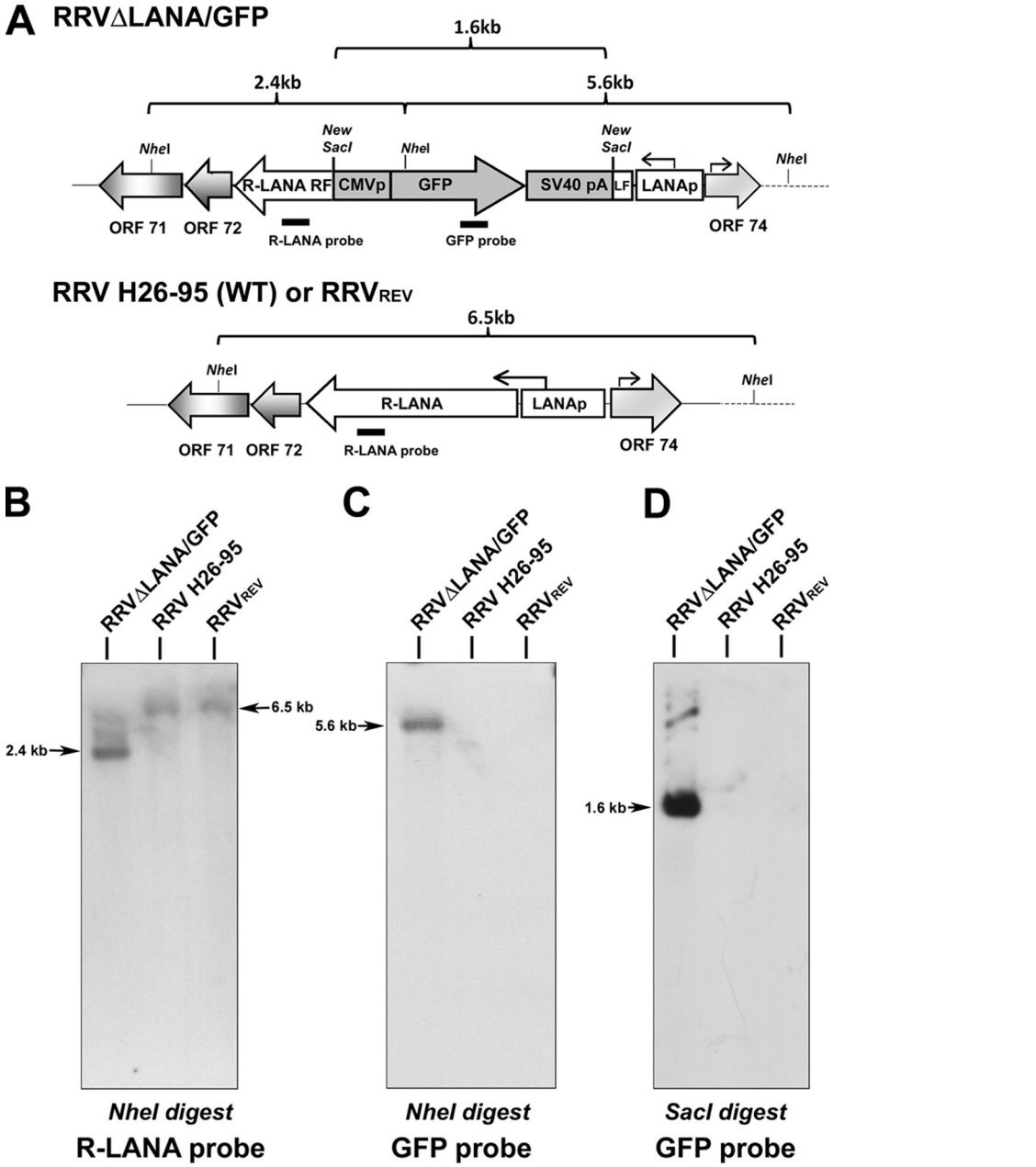

FIG. 3. Restriction digest and Southern blot analysis of recombinant viruses. (A) A schematic illustration showing the strategy for NheI or SacI restriction enzyme digestion and Southern blot analysis of RRVΔLANA/GFP, WT H26-95, and RRV_{REV} genomic DNA. R-LANA probe was generated from digestion of a plasmid encoding R-LANA, and the GFP probe was generated from a PCR product of the pEGFP-N1 plasmid. (B) The R-LANA probe hybridized to a 2.4-kb fragment in RRVΔLANA/GFP digested with NheI, and a 6.5-kb fragment in RRV H26-95 and RRV_{REV} digested with NheI. (C) The GFP probe hybridized to a 5.6-kb fragment of NheI-digested RRVΔLANA/GFP genomic DNA. The GFP probe did not hybridize to the WT H26-95 or RRV_{REV} DNA, as expected. (D) Restriction digestion with SacI released a 1.6-kb fragment corresponding to the size of the exogenous GFP sequence from RRVΔLANA/GFP genomic DNA, but no fragment was detected in the WT or revertant viral DNA.

rameters. Only reads of 35 nucleotides were used. We obtained 8,179,932 raw reads. A total of 1,451,388 reads matched the AF210726 RRV strain H25-95 sequence, excluding any gaps and allowing for at most one mismatch. Maximum coverage was 876-fold excluding the terminal repeats. The detailed coverage distribution is shown in Fig. 4A. Importantly, RRVΔLANA/GFP contained no deletions or rearrangements (average coverage per base pair >100). The RRVΔLANA/GFP genome is identical to the reference H26-95 sequence except at the disrupted R-LANA ORF. A few single nucleotide polymorphisms were present that were also polymorphic in the other RRV 17577 strain and may in fact represent sequencing errors in the initial reference sequence. Correct insertion of the GFP cassette into the R-

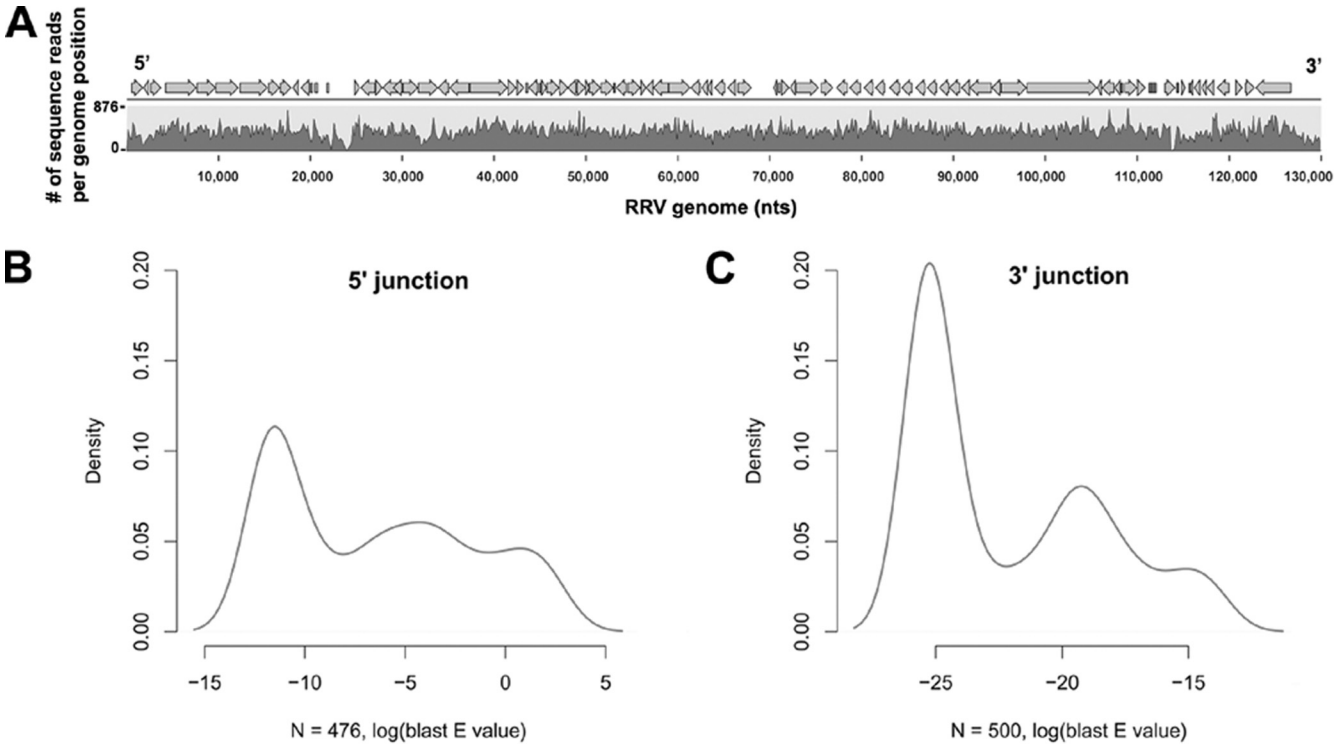

FIG. 4. Illumina/Solexa whole viral genome sequencing. (A) Coverage of RRVΔLANA/GFP genome by Solexa sequencing reads. Solexa generates 35-bp DNA reads. These were aligned to the RRV H26-95 genome using the reference sequence. The arrows on top represent individual RRV ORFs and the numbers represent nucleotide coordinates. The graph below shows the number of reads at each nucleotide position on a linear scale from 0 to 876. Peaks indicate regions of high coverage, valleys indicate regions of low coverage. Complete coverage of the whole RRV H26-95 genome was achieved. Maximum coverage was 876-fold. (B) Correct insertion of the GFP cassette into the R-LANA ORF was verified by comparing all Solexa fragments with the predicted RRV LANA-GFP junctional sequence. We found 476 Solexa reads that matched the 5′ LANA-GFP junctional sequence. Shown is the distribution (density) of BLAST scores log(blast E value) for this comparison. Lower values (i.e., those less than −10) indicate sequence reads that matched the junction sequence perfectly, without any gap or even a single mismatch. (**C**) We found 500 Solexa reads that matched the 5′ LANA-GFP junctional sequence. Shown is the distribution (density) of BLAST scores log(blast E value) for this comparison. Again, the majority of reads matched perfectly [lowest log(blast E value)]. If there was an inadvertent single nucleotide insertion at this site, we would expect the majority (i.e., the peak of the density distribution) not to be associated with the lowest log(blast E value) but with a higher one, indicative of a mismatch.

LANA ORF was verified by comparing the sequenced fragments to the predicted LANA-GFP junctional sequences (Fig. 4B and C). Importantly, 476 Illumina reads matched the 5′ junction without gaps or mismatch, and 500 reads matched the 3′ junction sequences without gaps or mismatch. This demonstrates that the recombinant virus had the desired structure and no inadvertent secondary mutations.

Absence of R-LANA leads to more lytic replication during de novo infection. As we have previously reported (18), RRV infection of RhF provides a lytic system for studying de novo viral replication. We wanted to examine the role of R-LANA in lytic replication in the context of the whole virus. Infection with RRVΔLANA/GFP, the parental H26-95 virus, revertant virus RRV_{REV}, and RRV-GFP viruses was performed at an MOI of 0.5 (Fig. 5), 0.1 (Fig. 6), or 5 (Fig. 7) in duplicate on confluent monolayers of RhF. These three different MOIs were chosen in order to assess whether R-LANA may have variegating effects on lytic viral replication based on multiple-step (MOIs of 0.1 and 0.5) versus single-step (MOI of 5) infection conditions. RRV-GFP virus (18) contains a CMV IE promoter-driven GFP cassette in a noncoding intergenic region of RRV between ORFs 18 and 19. RRV-GFP virus was used to control for any undesirable GFP-related effects on RRVΔLANA/GFP viral replication. After an inoculation period of 2 h for optimal adsorption, the supernatants from the infected cells were aspirated and replaced with DMEM containing 2% FBS to allow infections to proceed. At 0, 24, 48, 72, 96, 120, and 144 h postinfection, cell-free supernatants were harvested by centrifugation at 2,000 rpm for 5 min. For the viral growth curves, the supernatants were serially diluted in triplicate and subjected to traditional plaque assays to measure infectious particles (Fig. 5A, 6A, and 7A). For real-time PCR to measure extracellular viral genome copies (Fig. 5B, 6B, and 7B), 200 μl of the clarified supernatant for each infection sample, spiked with salmon sperm DNA, was processed through a DNeasy column (Qiagen) for DNA isolation. Then, 100 μl of the eluate was collected, 4 μl of which was subjected to real-time PCR in triplicate using a SYBR green mixture containing RRV Orf50 primers. To obtain absolute quantification, a standard curve for Orf50 was generated for each real-time PCR run. For QPCR intracellular viral assays, the infected cells were harvested by trypsinization. Each infected cell pellet was resuspended in 200 μl of PBS, and the total DNA content was column purified by using a DNeasy kit (Qia-

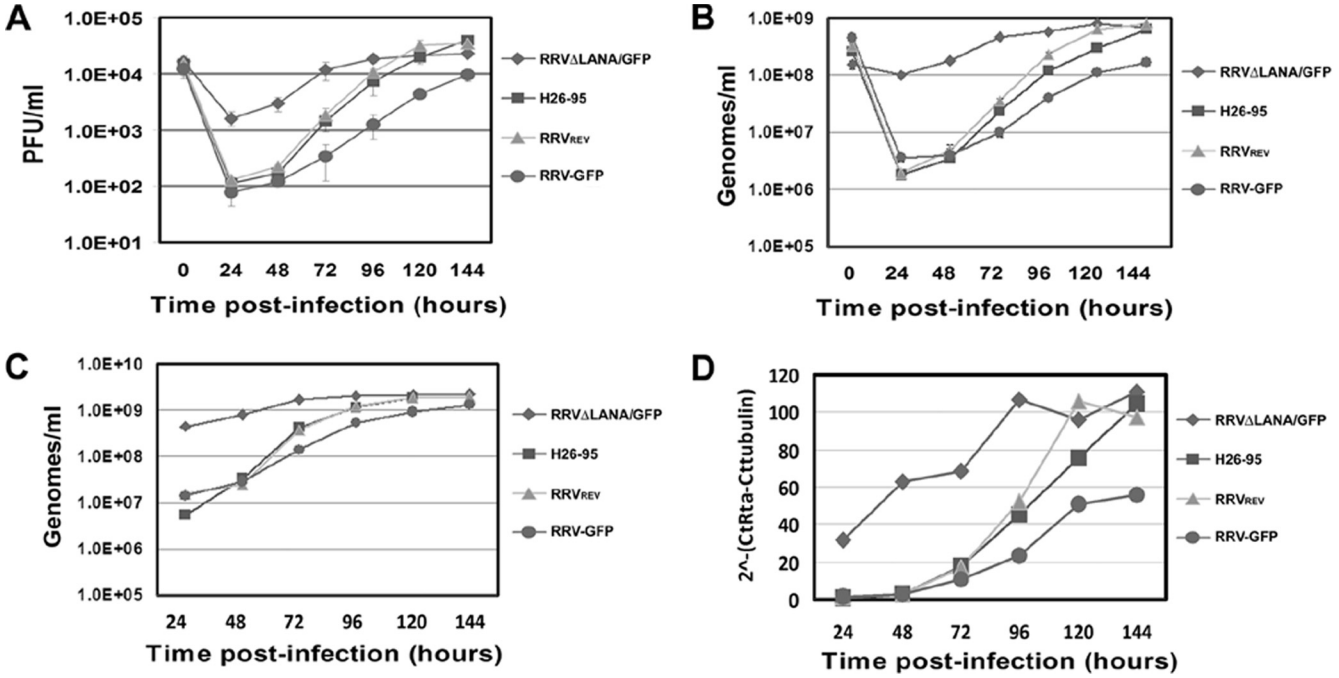

FIG. 5. Viral growth curves of RRVΔLANA/GFP in rhesus fibroblasts at an MOI of 0.5. Equivalent numbers of RhF cells were infected with RRVΔLANA/GFP, WT H26-95, RRV_{REV}, or RRV-GFP at an MOI of 0.5. Cell-free supernatants and cell pellets were harvested at indicated points postinfection. (A) Infectious virus particles from supernatants were quantitated by traditional plaque assay. (B) Extracellular viral genomes from the same samples as in panel A were quantitated by real-time PCR assay. In this real-time PCR-based assay, a RRV Orf50/Rta copy number standard curve was used to generate the viral genome copy number. (C) Intracellular viral genomes extracted from infected cell pellets were quantitated by real-time PCR using a RRV Orf50 standard curve to generate the viral genome copy number. (D) The viral genomes were normalized to rhesus β-tubulin copy numbers. The same samples as in panel C were subjected to real-time PCR with RRV Orf50 primers as described in panel C, and rhesus β-tubulin primers to absolutely quantitate rhesus β-tubulin copy numbers using a rhesus β-tubulin standard curve. During real-time QPCR, the amount of product at each cycle is quantified, and the C_T at which the product signal crossed a user-defined threshold is recorded. In this figure, dC_T is mathematically defined as $C_{T(\mathrm{Rta})} - C_{T(\mathrm{tubulin})}$, the signal difference between the viral gene Orf50 and the cellular gene rhesus β-tubulin in a sample. The *y* axis ($2^{CT(\mathrm{Rta}) - CT(\mathrm{tubulin})}$) thus reflects the fold difference, or relative abundance, of RRV viral genomes compared to the cellular genomes. In all panels, results are the averages of duplicate or triplicate samples. Error bars represent the standard deviations.

gen) and eluted in 200 μl of elution buffer. Then, 4 μl of the eluate was subjected to real-time QPCR in triplicate. The results are shown in Fig. 5C, 6C, and 7C. In order to account for cell death after viral replication in our data analysis, intracellular viral genomes were also normalized to rhesus genomes using rhesus tubulin as an endogenous control (Fig. 5D, 6D, and 7D).

The results at all three MOIs show that RRVΔLANA/GFP exhibited significantly faster growth kinetics by replicating to higher titers compared to the other three viruses. This enhanced growth property was more pronounced during earlier time points. At later time points, the levels of RRVΔLANA/GFP viral genomic DNA and RRVΔLANA/GFP infectious particles reached a plateau, whereas DNA synthesis of the parental H26-95 virus, revertant virus RRV_{REV}, and RRV-GFP continued. This was likely due to the depletion of viable cells available for replication of RRVΔLANA/GFP virus during later time points, after the virus had replicated through the monolayer of RhF at earlier time points. Expectedly, the rescue virus RRV_{REV} displayed growth kinetics nearly identical to those of WT RRV as determined by plaque assay and genome quantitation assay. As revealed by comparing the growth curves of RRV-GFP virus with the WT and revertant viruses, the presence of GFP slightly decreased virus replication at MOIs of both 0.1 and 0.5. This is likely due to the cytotoxic effects of GFP expression on the infected RhF. Thus, true assessment of the role of R-LANA on lytic viral replication should be made by comparing the viral growth curves of RRVΔLANA/GFP to that of the RRV-GFP recombinant virus. The RRVΔLANA/GFP virus showed a >10-fold-higher level of replication than the RRV-GFP virus at early time points. In addition, the RRVΔLANA/GFP virus produced more viral genomes and functional virions than the RRV-GFP virus at all time points at MOIs of both 0.1 and 0.5. At the single-step MOI of 5, the more rampant viral replication by RRVΔLANA/GFP was maintained during early infection up to 72 h postinfection and then plateaued due to the depletion of viable cells required for replication.

The absence of R-LANA results in the enhanced transcriptional expression of many RRV genes. Based on our growth curve experiments (Fig. 5, 6, and 7), RRVΔLANA/GFP virus displayed more lytic viral replication than the H26-95, RRV-GFP, and RRV_{REV} viruses. We were therefore interested in determining whether the overall pattern of RRV viral gene expression was altered during de novo infection. We used the RRV real-time quantitative PCR viral array our lab previously

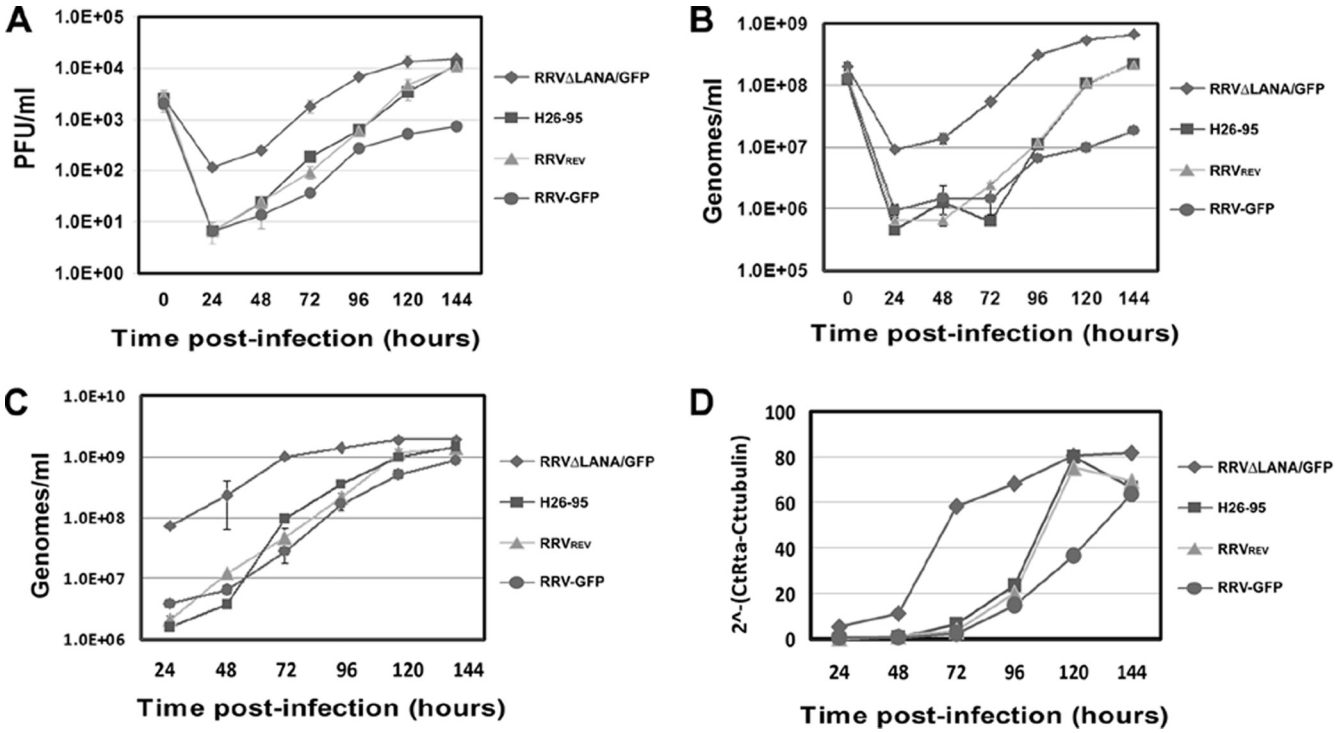

FIG. 6. Viral growth curves of RRVΔLANA/GFP in rhesus fibroblasts at an MOI of 0.1. Equivalent numbers of RhF cells were infected with RRVΔLANA/GFP, WT H26-95, RRV_{REV}, or RRV-GFP at an MOI of 0.1. Cell-free supernatants and the cell pellet were harvested at the indicated time points postinfection. (A) Infectious virus particles from supernatants were quantitated by traditional plaque assay. (B) Extracellular viral genomes from the same samples as in panel A were quantitated by real-time PCR assay. In this real-time PCR-based assay, a RRV Orf50 copy number standard curve was used to generate the viral genome copy number. (C) Intracellular viral genomes extracted from infected cell pellets were quantitated by real-time PCR using a RRV Orf50 standard curve to generate the viral genome copy number. (D) The viral genomes were normalized to rhesus β-tubulin copy numbers. The same samples as in panel C were subjected to real-time PCR with RRV Orf50 primers, as described in panel C, and rhesus β-tubulin primers to absolutely quantitate the rhesus β-tubulin copy numbers using a rhesus β-tubulin standard curve. In all of the panels, the results are the averages of duplicate or triplicate samples. Error bars represent the standard deviations.

reported (25) to profile the gene expression of all 84 RRV ORFs after de novo infection of RhF at an MOI of 0.5. A heat map representation of real-time QPCR data normalized to rhesus tubulin (dC_T) from viral infection time points at 0, 12, 24, 48, 72, 96, 120, and 144 h postinfection was generated. The dC_T values were subjected to hierarchical clustering using the standard Euclidian correlation method. Beginning at 24 h postinfection, the RRVΔLANA/GFP-infected cells displayed upregulation of the majority of viral genes of IE, early, and late classes compared to RRV-GFP-infected cells (Fig. 8A). A higher-resolution image of Fig. 8A is shown in Fig. S3 in the supplemental material. The upregulated RRV IE genes included Orf50/Rta. Furthermore, almost all of the RRV early genes (ORFs R1, 43, 6, 29a, 17, R9-1, 27, 24, 45, 55, R8, 74, 8, and 49) were robustly upregulated in the RRVΔLANA/GFP-infected cells compared to RRV-GFP-infected cells. Examples of upregulated late transcripts in the RRVΔLANA/GFP-infected cells are ORFs 25/MCP, 28/gp150, 29b (packaging protein), 32 (transport protein), 53/gN, R9-3/vIRF, 65/SCIP, 67, 67.5, 69, 75/vFGARAT, 23 (egress protein), and 9/polymerase. Unlike the IE and early genes, the extent of late gene upregulation in the RRVΔLANA/GFP-infected cells was not as robust. Indeed, among the late genes listed above, only Orf65/SCIP and Orf69 exhibited highly differential expression in the RRVΔLANA/GFP-infected cells compared to the RRV-GFP-infected cells. The remainder of the late transcript levels were only modestly increased in the RRVΔLANA/GFP-infected cells. Notably, infection with RRVΔLANA/GFP resulted in increased expression of all RRV Rta-responsive genes. These include R8, Orf8/gB, Orf57/MTA, whose expression we previously reported to be induced by RRV Orf50 transient expression using luciferase reporter constructs (17). Transcription of the RRV homologues of KSHV Rta-responsive viral genes (Orf6/ssDBP, R1, Orf9/DNApol, Orf74/vGPCR, and Orf45) was also found to be preferentially elevated in the RRVΔLANA/GFP-infected cells compared to RRV-GFP-infected cells. Taken together, these data suggest that RRV Rta function may be unchecked in the absence of R-LANA expression and that R-LANA has an impact on the expression of many RRV viral genes. Only a few RRV genes, including Orf38 and OrfR9-3/vIRF, did not show much R-LANA dependency in their expression profiles. Importantly, genetic disruption of R-LANA did not inhibit the transcription of the adjacent Orf71 and Orf72 genes. Orf72 gene expression was upregulated in the RRVΔLANA/GFP virus, suggesting that unimpeded Rta expression further enhances the R-LANA promoter for this transcript. Orf71 was also increased in the RRVΔLANA/GFP-infected cells but less dramatically than was Orf72. This result might be due to the predominant effect of the cryptic promoter for monocistronic Orf71 transcript

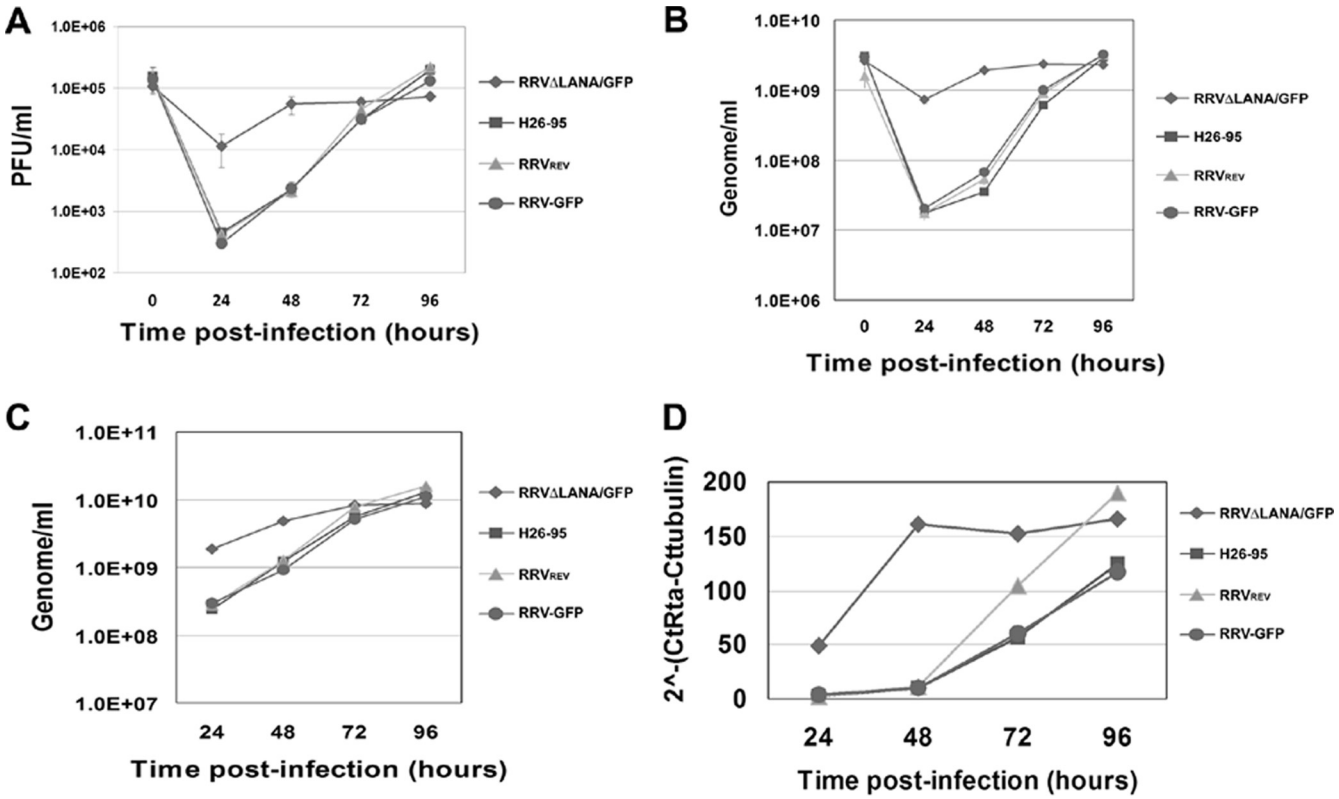

FIG. 7. Viral growth curves of RRVΔLANA/GFP in rhesus fibroblasts at an MOI of 5. Equivalent numbers of RhF cells were infected with RRVΔLANA/GFP, WT H26-95, RRV_{REV}, or RRV-GFP at an MOI of 5. Cell-free supernatants and cell pellet were harvested at indicated points postinfection. (A) Infectious virus particles from supernatants were quantitated by traditional plaque assay. (B) Extracellular viral genomes from the same samples as in panel A were quantitated by real-time PCR assay. In this real-time PCR-based assay, a RRV Orf50 copy number standard curve was used to generate the viral genome copy number. (C) Intracellular viral genomes extracted from infected cell pellets were quantitated by real-time PCR using a RRV Orf50 standard curve to generate the viral genome copy number. (D) The viral genomes were normalized to rhesus β-tubulin copy numbers. The same samples as in panel C were subjected to real-time PCR with RRV Orf50 primers, as described in panel C, and rhesus β-tubulin primers to absolutely quantitate rhesus β-tubulin copy numbers using a rhesus β-tubulin standard curve. In all of the panels, the results are the averages of duplicate or triplicate samples. Error bars represent the standard deviations.

driving Orf71 expression in an Rta-independent fashion during lytic replication as previously described (31). Our array also contained negative controls, including primers for KSHV genes (Orf73/LANA, Orf50/Rta, Orf57/MTA, K1, Orf74/vGPCR), human GAPDH (glyceraldehyde-3-phosphate dehydrogenase), human actin, and murine *apoB* genes. As expected, the expression of any KSHV, human, or mouse transcripts was undetectable in RRV-infected rhesus fibroblasts.

The QPCR primers amplified their respective targets efficiently and independent of the overall levels of any particular viral messages. This is visualized by plotting the log standard deviation [log(SD)] against the mean raw C_T values (Fig. 8B). No correlation was evident. Except for three outliers with mean C_Ts > 35, all data were within the linear range of the assay.

To quantitatively assess whether there was a difference in the transcription profile between the mutant and the WT, we calculated the difference ddC_T in mRNA levels for every mRNA at every time point, which is equivalent to taking the ratio of absolute mRNA levels between RRVΔLANA/GFP and RRV-GFP viruses. Next, we fitted a linear regression curve to the ddC_T over time and calculated the P value using the F statistic (29) to determine whether there was a linear trend over time. For any mRNA with no differences between the mutant and WT virus, ddC_T would be the same at each time point, and there would be no significant correlation. This is evidenced by tubulin, which has a P value of 0.76 (Fig. 8C). Note that this statistic is based on $n = 16$ data points. A few viral genes showed intermediate dependencies, but the majority of viral mRNAs ($n = 72$) exhibited a significant linear trend with a mean $P \leq 0.02$. We used q-value calculations (81) to adjust for multiple comparisons (Fig. 8D). This demonstrated that within our total set of 84 genes, we would expect at most 4 genes to show this trend by chance alone. Since we observed 72 genes, this analysis establishes that there is a significant difference between WT and recombinant virus mRNA levels and that almost all mRNA transcripts of the RRVΔLANA/GFP were transcribed at higher levels at earlier times than the WT virus.

R-LANA modulates the transcription of cellular genes. We also examined several cellular genes that are known to be repressed by KSHV LANA in the context of lytic infection with the RRVΔLANA/GFP and RRV-GFP viruses. In brief, RhF were infected with either virus (MOI of 1) for 48 h. Total RNA was isolated from infected RhF, and 1 μg of the RNA was reverse transcribed using the Promega reverse transcription

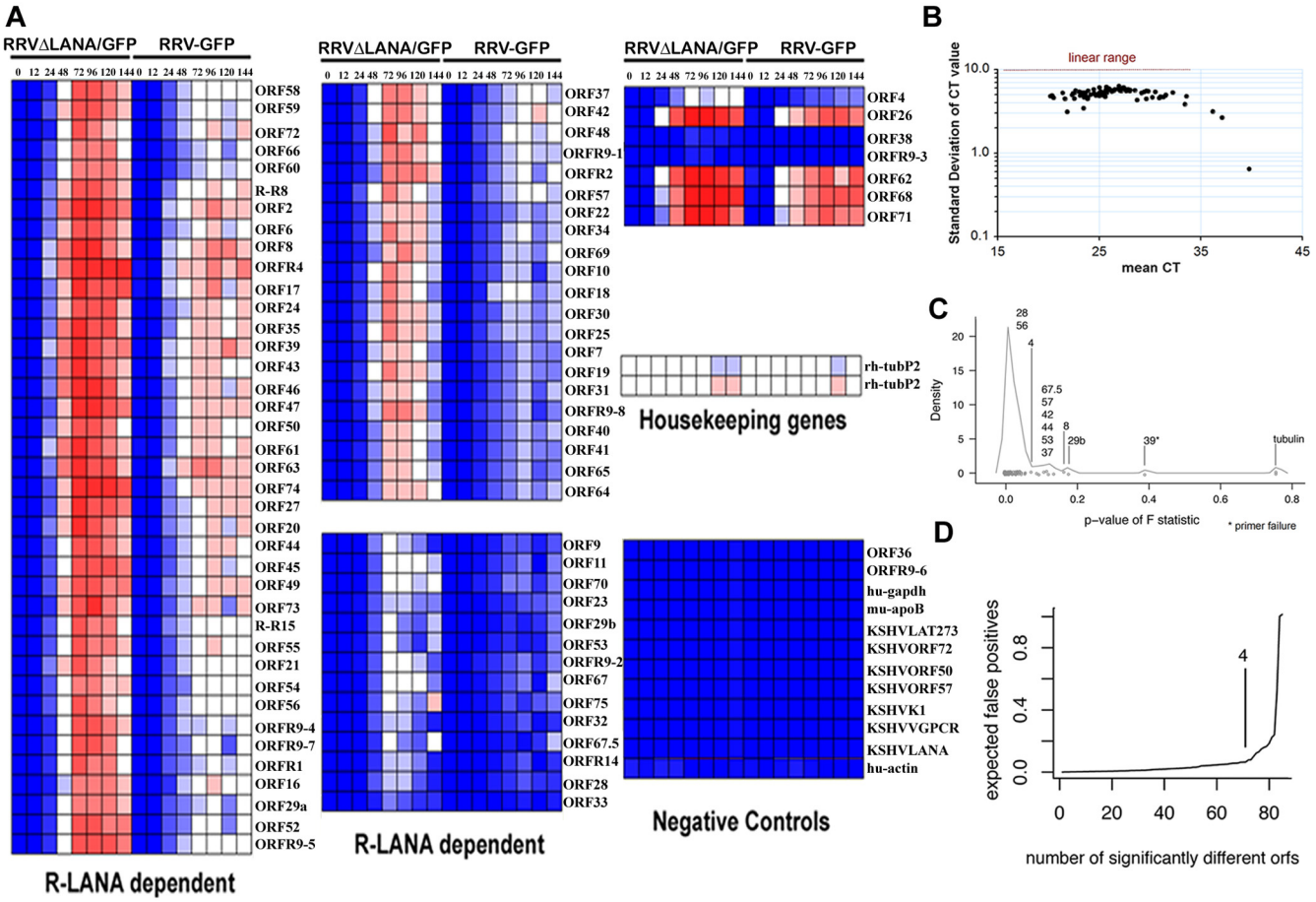

FIG. 8. Viral gene profiling of RRVΔLANA/GFP and RRV-GFP-infected rhesus fibroblasts. (A) Heat map representation of real-time QPCR data normalized to rhesus tubulin (dC_T) of infected cells obtained at 0, 12, 24, 48, 72, 96, 120, and 144 h postinfection. The dC_T values were hierarchically clustered by using standard Euclidian correlation method. Blue indicates low, white represents intermediate/median, and red represents the highest level of viral mRNA detected relative to rhesus tubulin. (See Fig. S3 in the supplemental material for a high-resolution image.) (B) Quality control of RRV QPCR primers for all of the ORFs. There was no significant correlation between the magnitude of the log(SD) and the mean C_T, demonstrating that, except for three outliers, changes in RRV gene expression did not depend on the overall levels of any particular viral mRNA. (C) Distribution of RRV ORFs showing differential transcript abundance between samples. We determined for each individual gene in the array whether its relative abundance at each time point differed between the WT and the mutant. The significance of the difference is expressed by the *P* value of the F statistic. mRNAs that differed significantly in their transcription pattern yield a low *P* value. We then plotted the density, i.e., the distribution of *P* values for all mRNAs in the array. Individual dots just above the *x* axis indicate individual mRNAs. The peak at a low *P* value indicates that the majority of mRNAs have differential expression between the WT RRV-GFP and mutant RRVΔLANA/GFP viruses. Orf4 has a *P* value of 0.076 and is a watershed to differentiate ORFs that exhibit statistically significant differences (peak group left to Orf4) from those that do not (right to Orf4). Orf28 and Orf56 are the only genes within the peak group with a *P* of >0.05. (D) A great concern in array analysis is the problem of multiple comparisons. Given enough comparisons; one would expect some ORFs to show a statistically significant difference by chance alone. These are called false positives. The expected number of false positives (i.e., the rate) can be calculated based on the total number of genes in the array and the *P* values of the individual comparisons. Shown in this panel is a plot of the expected rate of false positives against the number of RRV ORFs considered showing individually statistically significant differences in mRNA levels between WT and mutant viruses. Based on the *P* value distribution in panel C, one would expect less than 1 (<0.02) false positive within the top 71 differentially regulated genes, i.e., those that differed more significantly between the WT and mutant than Orf4 (indicated in panel D).

system and oligo(dT) primers. The cDNA was then subjected to real-time PCR using standard cycling conditions with primers specific to genes that were previously cited to be repressed by LANA (Table 1). The real-time PCR primers are shown in Table 2. In real-time PCR, higher C_T values correlate with a lower abundance of the examined RNA and vice versa. A dC_T value is defined as the C_T value of each listed gene minus the C_T value of the endogenous control, rhesus β-tubulin. A negative dC_T value indicates a higher expression level of the specific gene compared to the control rhesus β-tubulin gene. The C_T value for each gene (including β-actin, which was used as another endogenous control) was normalized to the C_T value of rhesus β-tubulin from the same sample to generate dC_T ($dC_T = C_{T(\text{gene of interest})} - C_{T(\beta\text{-tubulin})}$) values for mock, RRVΔLANA/GFP and RRV-GFP-infected cells (Table 1). A ddC_T value is defined as the dC_T value of each listed gene from an infected sample minus the dC_T value of the same gene from a mock-infected sample. The ddC_T values were calculated for RRVΔLANA/GFP compared to mock infection and for RRV-GFP compared to mock infection, respectively. The fold acti-

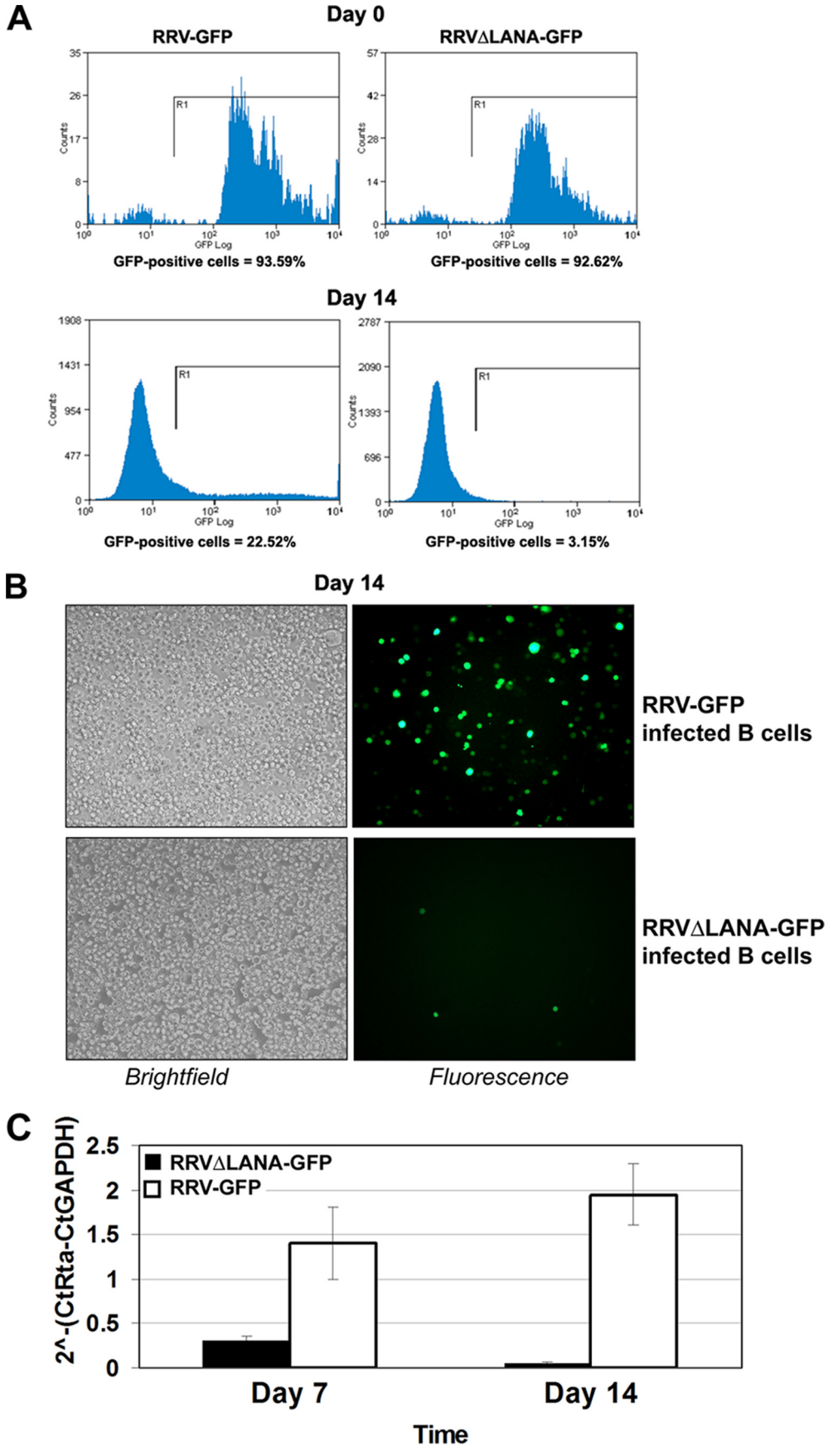
A
Day 0
RRV-GFP
RRVΔLANA-GFP
R1
Counts
GFP Log
GFP-positive cells = 93.59%
GFP-positive cells = 92.62%
Day 14
GFP-positive cells = 22.52%
GFP-positive cells = 3.15%
B
Day 14
RRV-GFP infected B cells
RRVΔLANA-GFP infected B cells
Brightfield
Fluorescence
C
2^-(CtRta-CtGAPDH)
RRVΔLANA-GFP
RRV-GFP
Day 7
Day 14
Time

vation of the specific gene in RRVΔLANA/GFP-infected cells compared to RRV-GFP-infected cells was subsequently deduced and is shown in Table 1. Previous reports have shown that KSHV LANA can repress nuclear receptor coactivator 3 (NCOA3), cyclic AMP (cAMP) responsive element binding protein-like 1 (CREBL1), CCAAT-box binding transcription factor, G_1/S-specific cyclin-D2 (CCND2), and forkhead box protein G1B (FKHL1/FOXG1B) when expressed in isolation in B cells or endothelial cells (2, 3, 51). We found that these genes are derepressed, i.e., activated during de novo lytic infection of RhF with the RRVΔLANA/GFP virus compared to RRV-GFP (Table 1). The β-actin gene serves as a control since its expression did not change in cells infected with either RRVΔLANA/GFP or RRV-GFP. Specifically, An et al. showed that the transcriptional factors NCOA3, CREBL1, and CCAAT-box binding transcription factor were downregulated between 2- and 4.9-fold when LANA expression was induced by doxycycline in BJAB/Tet-On/LANA cells (2). Our data using the RRVΔLANA/GFP virus suggest that R-LANA might also repress the transactivation of cellular and/or viral genes that are dependent on these transcription factors. Since NCOA3 has an intrinsic histone acetyltransferase (HAT) activity (10), one might also speculate that LANA suppression of NCOA3 gene expression could lead to histone remodeling in order to silence genes that are normally activated by NCOA3. Moreover, Shamay et al. previously demonstrated that expression of KSHV LANA in TIME endothelial cells resulted in a strong repression of FKHL1/FOXG1B (17-fold) and CCND2 (4.6-fold) gene expression (77). Such repression was due to LANA recruitment of the methyltransferase Dnm3ta and could be reversed by using a methyltransferase inhibitor (77). Our finding that the RRVΔLANA/GFP virus-infected cells display higher activation of FKHL1/FOXG1B and CCND2 gene expression than the RRV-GFP-infected cells suggests that R-LANA does indeed repress FKHL1/FOXG1B and CCND2 gene expression, even in the context of the whole virus. This finding also suggests an epigenetic mechanism for R-LANA-mediated silencing of cellular genes and further corroborates LANA's role in suppressing gene transcription (77).

R-LANA is important for establishment of latency in BJAB cells. We determined whether R-LANA also modulates the establishment and maintenance of RRV in B cells. To address this question, we infected BJAB B cells with RRVΔLANA/GFP or RRV-GFP (MOI of 0.5) as previously described (18). At 7 days postinfection, infected BJAB cells were sorted by flow cytometry for the presence of green fluorescence. RRVΔLANA/GFP showed higher infectivity of BJAB cells than RRV-GFP on day 0 presorting (data not shown). After sorting, we used equivalent numbers of GFP-positive cells from both RRVΔLANA/GFP-infected and RRV-GFP-infected BJAB cells for further experimentation (Fig. 9A, upper panels). From here onward, BJAB cells were split every 2 days, and GFP-positive cells were continuously monitored by fluorescence microscopy and flow cytometry. The RRVΔLANA/GFP-infected BJAB sample showed a rapid loss of GFP-positive cells on days 7 and 14 postsorting, as determined by fluorescence microscopy and flow cytometry. Figure 9A (lower panels) and Fig. 9B show the relative GFP-positive cells on day 14 postsorting, as determined quantitatively by flow sorting and visually by fluorescence microscopy, respectively. To confirm that the dramatic decrease in GFP-positive cells in RRVΔLANA/GFP-infected BJAB cells was due to the loss of RRV particles (or intracellular viral genomes), we performed real-time QPCR to calculate the RRV genome copy number. RRVΔLANA/GFP-infected BJAB cells displayed significantly lower intracellular viral genomes than did RRV-GFP-infected BJAB cells (Fig. 9C).

DISCUSSION

KSHV LANA (K-LANA) has been extensively studied in regard to its molecular functions in regulating cell cycle, apoptosis, and immune evasion, as well as viral latency (reviewed in references 21 and 84). By comparison, relatively little is known about R-LANA. Given our previous finding that R-LANA can inhibit RRV Rta-mediated transactivation of a subset of lytic viral genes (16), we hypothesized that an R-LANA deletion mutant virus would display dysregulated transcription compared to WT RRV. We report here the use of homologous recombination to generate RRVΔLANA/GFP and a revertant RRV_{REV} recombinant virus to gain insight into the replication kinetics of the R-LANA knockout virus. We found that RRVΔLANA/GFP displayed increased lytic activity when the R-LANA ORF was functionally disrupted by the insertion of a GFP expression cassette. By generating viral growth curves using traditional plaque assays, as well as QPCR viral load assays, we demonstrated increased production of both viral genomes by real-time QPCR, and infectious virion particles by plaque assay, in RRVΔLANA/GFP-infected RhF compared to WT and RRV-GFP-infected RhF. Furthermore, whole-genome profiling of RRV transcripts provided an unbiased scrutiny of all RRV lytic gene expression that was altered by the functionally disrupted R-LANA, suggesting that the observed increase in RRV lytic activity was caused by global upregulation of RRV mRNA transcripts. Because Orf50/Rta is necessary and sufficient for the initiation and orchestration of the

FIG. 9. RRVΔLANA/GFP and RRV-GFP infection of B lymphocytes. The KSHV-negative PEL cell line, BJAB, was infected with RRVΔLANA/GFP or RRV-GFP virus at an MOI of 0.5 by spinoculation. At 7 days postinfection, infected BJAB cells were sorted by flow cytometry for the presence of green fluorescence. (A) Flow cytometry analysis of GFP-positive BJAB cells infected with RRVΔLANA/GFP or RRV-GFP virus immediately after sorting (day 0 postsorting) and 14 days postsorting. The percentages of GFP-positive cells at the indicated time points are shown below the graphs. (B) Representative images of RRVΔLANA/GFP and RRV-GFP-infected BJAB cells on day 14 postsorting. Bright-field and GFP fluorescence images of RRV-infected GFP-positive B cells are shown. (C) Intracellular viral genomes of RRVΔLANA/GFP (■)- and RRV-GFP (□)-infected BJAB cells on day 7 and day 14 postsorting. Intracellular genomes extracted from infected cell pellets were quantitated by real-time PCR using a RRV Orf50 standard curve to generate the viral genome copy number. The viral genomes were normalized to human GAPDH copy numbers, which were generated by using a human GAPDH standard curve. The results are the averages of triplicate samples. Error bars represent the standard deviations.

lytic viral transcriptional cascade, we speculate that the lytic behavior of RRVΔLANA/GFP in our permissive RhF tissue culture system was largely due to unhampered Rta transactivation activity when R-LANA expression was lost. Thus, R-LANA plays a pivotal role in suppressing lytic replication during de novo infection.

Several possible mechanisms could explain how R-LANA might inhibit Rta transactivation of Rta-responsive genes. The most obvious explanation is chromatin remodeling, as R-LANA has been implicated in recruiting histone deacetylases (16), the result of which may lead to histone modification of Rta-responsive viral promoters. Such a mechanism has also been proposed for K-LANA by physical interaction with RBP-Jκ and other cellular proteins (20, 45, 52, 53). In addition, Lu et al. reported that Orf50 transcription is specifically repressed by KSHV LANA during viral latency (52). In dually infected PELs, K-LANA has been shown to suppress EBV genes by regulating the mSin3 corepressor complex (43), although K-LANA was also reported to activate EBV or human immunodeficiency virus genes (30, 34), as well as cellular genes (4, 40, 83). The transcriptional activation and repression activities have been mapped to the amino and carboxyl termini of K-LANA, respectively (61, 75, 86). In addition to recruiting histone deacetylases for transcription repression, as we previously published (16), R-LANA might sequester HATs from Rta or Rta-dependent viral promoters. Our finding that R-LANA decreased the gene expression of the HAT, NCOA3, suggests that R-LANA might also repress HAT-mediated transcription.

In KSHV, both LANA and Rta have been shown to bind CREB-binding protein, which has HAT activity and can activate transcription (32, 48, 49). Other possibilities by which R-LANA could inhibit Rta function include affecting Rta protein levels and modification of Rta posttranslationally in order to downregulate Rta transactivation function. Our preliminary data have excluded these two possibilities (unpublished data). Interestingly, a significant number of RRV genes that were upregulated in the RRVΔLANA/GFP-infected cells compared to the RRV-GFP-infected cells have not been previously identified as being Rta-responsive in either the KSHV or RRV viral systems. KSHV LANA has been shown to act as a transcriptional repressor on some cellular promoters such as those that are dependent on CREB-binding protein or E2F transactivation (48, 49, 64, 66). It is therefore plausible that R-LANA acts as a direct transcriptional repressor of a subset of viral genes, independent of its inhibition of Rta transactivation.

As we were preparing the manuscript for submission, the characterization of a KSHVΔLANA virus in the context of lytic replication was published (47). These investigators reported that deletion of KSHV LANA resulted in the increased production of KSHV infectious virions after TPA and sodium butyrate treatment of KSHVΔLANA-infected cells, as well as enhanced transcription of the four Rta-responsive lytic genes MTA, Orf59, viral interleukin-6, and Orf-K8.1 (47). The expression of these homologous genes in RRV was also increased by RRVΔLANA/GFP de novo infection of RhF, and increased production of infectious RRV virions was also observed with RRVΔLANA/GFP infection compared to RRV-GFP infection. Importantly, this differential pattern of gene expression was seen in the absence of exogenous artificial inducers such as TPA and butyrate (47).

Furthermore, our study showed for the first time that LANA modulates transcription of cellular genes during lytic infection and in the context of the whole virus. Cellular genes such as NCOA3, CREBL1, CCAAT-box binding transcription factor, CCND2, and FKHL1/FOXG1B, which were previously reported to be repressed by KSHV LANA in either B cells or endothelial cells (2, 3, 51), were found to be derepressed in cells infected with RRVΔLANA/GFP compared to RRV-GFP.

A common property shared by KSHV, RRV, and MHV68 recombinant viruses with LANA deleted is that they exhibit dysregulated lytic gene expression. In replication assays, deletion of LANA from KSHV and deletion of LANA from RRV showed similar effects, i.e, increased replication of the LANA mutant viruses in vitro compared to that of the WT virus. However, deletion of LANA from MHV68 displayed no difference in replication in vitro at a high MOI and reduced virus titers compared to that for the WT virus at a very low MOI upon de novo infection of primary murine embryonic fibroblasts or HIN 3T3 fibroblasts (26, 27, 47, 57). This paradoxical observation could be attributed to differences in the cell lines being used in the replication assays or differences in the primate and murine LANA proteins.

Finally, RRVΔLANA/GFP was inefficient in establishing latency in infected BJAB cells. This was similar to what was observed with the KSHV LANA deletion mutant BAC36-ΔLNA, which failed to establish a latent infection in transfected human 293 cells (89).

A future goal of our study is to investigate RRVΔLANA/GFP infection in rhesus macaques to determine its behavior in vivo. In the case of the MHV68 LANA deletion virus, previous reports suggest that the loss of LANA resulted in a compromised ability of the virus to replicate in the lungs and establish latency in the spleen of infected mice (27, 57).

In conclusion, we have created a RRVΔLANA/GFP that is more lytic than RRV-GFP, WT RRV H26-95, or a revertant RRV_{REV} virus. This recombinant virus displays higher viral loads in rhesus fibroblasts, as well as increased expression of a multitude of RRV viral genes during lytic replication in rhesus fibroblasts. In addition, cellular genes that are normally repressed by LANA are derepressed in RRVΔLANA/GFP-infected cells compared to RRV-GFP-infected cells. Furthermore, the RRVΔLANA/GFP recombinant virus also fails to successfully establish latent infection in B lymphocytes.

ACKNOWLEDGMENTS

We thank Stuart Krall for assistance with the virus amplification. We are grateful to Chelsey Hilscher for technical contributions to the RRV QPCR array data and Melissa Wills for providing the rhesus tubulin plasmid. We thank members of the Damania and Dittmer lab for informative discussions. We also thank the UNC Genomics Facility for performing Solexa sequencing of the recombinant virus.

This study was supported by NIH grants CA096500 and DE018281 to B.D. and CA109232 to D.P.D. K.W.W. was supported in part by NIAID training grant T32-AI007001 and MSTP grant T32-GM008719. B.D. is a Leukemia and Lymphoma Society Scholar and Burroughs Welcome Fund Investigator in Infectious Disease.

REFERENCES

1. **Alexander, L., L. Denekamp, A. Knapp, M. R. Auerbach, B. Damania, and R. C. Desrosiers.** 2000. The primary sequence of rhesus monkey rhadinovirus

isolate 26-95: sequence similarities to Kaposi's sarcoma-associated herpesvirus and rhesus monkey rhadinovirus isolate 17577. J. Virol. **74:**3388–3398.
2. **An, F. Q., N. Compitello, E. Horwitz, M. Sramkoski, E. S. Knudsen, and R. Renne.** 2005. The latency-associated nuclear antigen of Kaposi's sarcoma-associated herpesvirus modulates cellular gene expression and protects lymphoid cells from p16 INK4A-induced cell cycle arrest. J. Biol. Chem. **280:** 3862–3874.
3. **An, J., Y. Sun, and M. B. Rettig.** 2004. Transcriptional coactivation of c-Jun by the KSHV-encoded LANA. Blood **103:**222–228.
4. **Bajaj, B. G., S. C. Verma, K. Lan, M. A. Cotter, Z. L. Woodman, and E. S. Robertson.** 2006. KSHV encoded LANA upregulates Pim-1 and is a substrate for its kinase activity. Virology **351:**18–28.
5. **Ballestas, M. E., P. A. Chatis, and K. M. Kaye.** 1999. Efficient persistence of extrachromosomal KSHV DNA mediated by latency-associated nuclear antigen. Science **284:**641–644.
6. **Barbera, A. J., J. V. Chodaparambil, B. Kelley-Clarke, V. Joukov, J. C. Walter, K. Luger, and K. M. Kaye.** 2006. The nucleosomal surface as a docking station for Kaposi's sarcoma herpesvirus LANA. Science **311:**856–861.
7. **Barbera, A. J., J. V. Chodaparambil, B. Kelley-Clarke, K. Luger, and K. M. Kaye.** 2006. Kaposi's sarcoma-associated herpesvirus LANA hitches a ride on the chromosome. Cell Cycle **5:**1048–1052.
8. **Cesarman, E., Y. Chang, P. S. Moore, J. W. Said, and D. M. Knowles.** 1995. Kaposi's sarcoma-associated herpesvirus-like DNA sequences in AIDS-related body-cavity-based lymphomas. N. Engl. J. Med. **332:**1186–1191.
9. **Chang, Y., E. Cesarman, M. S. Pessin, F. Lee, J. Culpepper, D. M. Knowles, and P. S. Moore.** 1994. Identification of herpesvirus-like DNA sequences in AIDS-associated Kaposi's sarcoma. Science **266:**1865–1869.
10. **Chen, H., R. J. Lin, R. L. Schiltz, D. Chakravarti, A. Nash, L. Nagy, M. L. Privalsky, Y. Nakatani, and R. M. Evans.** 1997. Nuclear receptor coactivator ACTR is a novel histone acetyltransferase and forms a multimeric activation complex with P/CAF and CBP/p300. Cell **90:**569–580.
11. **Cotter, M. A., II, and E. S. Robertson.** 1999. The latency-associated nuclear antigen tethers the Kaposi's sarcoma-associated herpesvirus genome to host chromosomes in body cavity-based lymphoma cells. Virology **264:**254–264.
12. **Cotter, M. A., II, C. Subramanian, and E. S. Robertson.** 2001. The Kaposi's sarcoma-associated herpesvirus latency-associated nuclear antigen binds to specific sequences at the left end of the viral genome through its carboxy terminus. Virology **291:**241–259.
13. **Damania, B., M. DeMaria, J. U. Jung, and R. C. Desrosiers.** 2000. Activation of lymphocyte signaling by the R1 protein of rhesus monkey rhadinovirus. J. Virol. **74:**2721–2730.
14. **Damania, B., M. Li, J. K. Choi, L. Alexander, J. U. Jung, and R. C. Desrosiers.** 1999. Identification of the R1 oncogene and its protein product from the rhadinovirus of rhesus monkeys. J. Virol. **73:**5123–5131.
15. **Desrosiers, R. C., V. G. Sasseville, S. C. Czajak, X. Zhang, K. G. Mansfield, A. Kaur, R. P. Johnson, A. A. Lackner, and J. U. Jung.** 1997. A herpesvirus of rhesus monkeys related to the human Kaposi's sarcoma-associated herpesvirus. J. Virol. **71:**9764–9769.
16. **DeWire, S. M., and B. Damania.** 2005. The latency-associated nuclear antigen of rhesus monkey rhadinovirus inhibits viral replication through repression of Orf50/Rta transcriptional activation. J. Virol. **79:**3127–3138.
17. **DeWire, S. M., M. A. McVoy, and B. Damania.** 2002. Kinetics of expression of rhesus monkey rhadinovirus (RRV) and identification and characterization of a polycistronic transcript encoding the RRV Orf50/Rta, RRV R8, and R8.1 genes. J. Virol. **76:**9819–9831.
18. **DeWire, S. M., E. S. Money, S. P. Krall, and B. Damania.** 2003. Rhesus monkey rhadinovirus (RRV): construction of a RRV-GFP recombinant virus and development of assays to assess viral replication. Virology **312:** 122–134.
19. **Dezube, B. J., M. Zambela, D. R. Sage, J. F. Wang, and J. D. Fingeroth.** 2002. Characterization of Kaposi sarcoma-associated herpesvirus/human herpesvirus-8 infection of human vascular endothelial cells: early events. Blood **100:**888–896.
20. **Di Bartolo, D. L., M. Cannon, Y. F. Liu, R. Renne, A. Chadburn, C. Boshoff, and E. Cesarman.** 2008. KSHV LANA inhibits TGF-beta signaling through epigenetic silencing of the TGF-β type II receptor. Blood **111:**4731–4740.
21. **Dittmer, D.** 2008. KSHV viral latent lifecycle, p. 495–520. *In* B. Damania and J. Pipas (ed.), DNA tumor viruses. Springer-Verlag, New York, NY.
22. **Dittmer, D., M. Lagunoff, R. Renne, K. Staskus, A. Haase, and D. Ganem.** 1998. A cluster of latently expressed genes in Kaposi's sarcoma-associated herpesvirus. J. Virol. **72:**8309–8315.
23. **Dittmer, D., C. Stoddart, R. Renne, V. Linquist-Stepps, M. E. Moreno, C. Bare, J. M. McCune, and D. Ganem.** 1999. Experimental transmission of Kaposi's sarcoma-associated herpesvirus (KSHV/HHV-8) to SCID-hu Thy/Liv mice. J. Exp. Med. **190:**1857–1868.
24. **Dittmer, D. P.** 2003. Transcription profile of Kaposi's sarcoma-associated herpesvirus in primary Kaposi's sarcoma lesions as determined by real-time PCR arrays. Cancer Res. **63:**2010–2015.
25. **Dittmer, D. P., C. M. Gonzalez, W. Vahrson, S. M. DeWire, R. Hines-Boykin, and B. Damania.** 2005. Whole-genome transcription profiling of rhesus monkey rhadinovirus. J. Virol. **79:**8637–8650.
26. **Forrest, J. C., C. R. Paden, R. D. Allen III, J. Collins, and S. H. Speck.** 2007. ORF73-null murine gammaherpesvirus 68 reveals roles for mLANA and p53 in virus replication. J. Virol. **81:**11957–11971.
27. **Fowler, P., S. Marques, J. P. Simas, and S. Efstathiou.** 2003. ORF73 of murine herpesvirus-68 is critical for the establishment and maintenance of latency. J. Gen. Virol. **84:**3405–3416.
28. **Gessain, A., A. Sudaka, J. Briere, N. Fouchard, M. A. Nicola, B. Rio, M. Arborio, X. Troussard, J. Audouin, J. Diebold, and G. de The.** 1996. Kaposi sarcoma-associated herpes-like virus (human herpesvirus type 8) DNA sequences in multicentric Castleman's disease: is there any relevant association in non-human immunodeficiency virus-infected patients? Blood **87:**414–416.
29. **Glanz, S. A.** 1992. Primer of biostatistics, 3rd ed. McGraw-Hill, New York, NY.
30. **Groves, A. K., M. A. Cotter, C. Subramanian, and E. S. Robertson.** 2001. The latency-associated nuclear antigen encoded by Kaposi's sarcoma-associated herpesvirus activates two major essential Epstein-Barr virus latent promoters. J. Virol. **75:**9446–9457.
31. **Grundhoff, A., and D. Ganem.** 2001. Mechanisms governing expression of the v-FLIP gene of Kaposi's sarcoma-associated herpesvirus. J. Virol. **75:** 1857–1863.
32. **Gwack, Y., H. Byun, S. Hwang, C. Lim, and J. Choe.** 2001. CREB-binding protein and histone deacetylase regulate the transcriptional activity of Kaposi's sarcoma-associated herpesvirus open reading frame 50. J. Virol. **75:** 1909–1917.
33. **Hu, J., A. C. Garber, and R. Renne.** 2002. The latency-associated nuclear antigen of Kaposi's sarcoma-associated herpesvirus supports latent DNA replication in dividing cells. J. Virol. **76:**11677–11687.
34. **Hyun, T. S., C. Subramanian, M. A. Cotter II, R. A. Thomas, and E. S. Robertson.** 2001. Latency-associated nuclear antigen encoded by Kaposi's sarcoma-associated herpesvirus interacts with Tat and activates the long terminal repeat of human immunodeficiency virus type 1 in human cells. J. Virol. **75:**8761–8771.
35. **Jeong, J., J. Papin, and D. Dittmer.** 2001. Differential regulation of the overlapping Kaposi's sarcoma-associated herpesvirus vGCR (Orf74) and LANA (Orf73) promoters. J. Virol. **75:**1798–1807.
36. **Jeong, J. H., J. Orvis, J. W. Kim, C. P. McMurtrey, R. Renne, and D. P. Dittmer.** 2004. Regulation and autoregulation of the promoter for the latency-associated nuclear antigen of Kaposi's sarcoma-associated herpesvirus. J. Biol. Chem. **279:**16822–16831.
37. **Kaleeba, J. A., E. P. Bergquam, and S. W. Wong.** 1999. A rhesus macaque rhadinovirus related to Kaposi's sarcoma-associated herpesvirus/human herpesvirus 8 encodes a functional homologue of interleukin-6. J. Virol. **73:** 6177–6181.
38. **Kelley-Clarke, B., M. E. Ballestas, T. Komatsu, and K. M. Kaye.** 2007. Kaposi's sarcoma herpesvirus C-terminal LANA concentrates at pericentromeric and peri-telomeric regions of a subset of mitotic chromosomes. Virology **357:**149–157.
39. **Kelley-Clarke, B., M. E. Ballestas, V. Srinivasan, A. J. Barbera, T. Komatsu, T. A. Harris, M. Kazanjian, and K. M. Kaye.** 2007. Determination of Kaposi's sarcoma-associated herpesvirus C-terminal latency-associated nuclear antigen residues mediating chromosome association and DNA binding. J. Virol. **81:**4348–4356.
40. **Knight, J. S., M. A. Cotter II, and E. S. Robertson.** 2001. The latency-associated nuclear antigen of Kaposi's sarcoma-associated herpesvirus transactivates the telomerase reverse transcriptase promoter. J. Biol. Chem. **276:** 22971–22978.
41. **Komatsu, T., M. E. Ballestas, A. J. Barbera, and K. M. Kaye.** 2002. The KSHV latency-associated nuclear antigen: a multifunctional protein. Front. Biosci. **7:**d726–d730.
42. **Komatsu, T., A. J. Barbera, M. E. Ballestas, and K. M. Kaye.** 2001. The Kaposi' s sarcoma-associated herpesvirus latency-associated nuclear antigen. Viral Immunol. **14:**311–317.
43. **Krithivas, A., D. B. Young, G. Liao, D. Greene, and S. D. Hayward.** 2000. Human herpesvirus 8 LANA interacts with proteins of the mSin3 corepressor complex and negatively regulates Epstein-Barr virus gene expression in dually infected PEL cells. J. Virol. **74:**9637–9645.
44. **Lagunoff, M., J. Bechtel, E. Venetsanakos, A. M. Roy, N. Abbey, B. Herndier, M. McMahon, and D. Ganem.** 2002. De novo infection and serial transmission of Kaposi's sarcoma-associated herpesvirus in cultured endothelial cells. J. Virol. **76:**2440–2448.
45. **Lan, K., D. A. Kuppers, S. C. Verma, N. Sharma, M. Murakami, and E. S. Robertson.** 2005. Induction of Kaposi's sarcoma-associated herpesvirus latency-associated nuclear antigen by the lytic transactivator RTA: a novel mechanism for establishment of latency. J. Virol. **79:**7453–7465.
46. **Langlais, C. L., J. M. Jones, R. D. Estep, and S. W. Wong.** 2006. Rhesus rhadinovirus R15 encodes a functional homologue of human CD200. J. Virol. **80:**3098–3103.
47. **Li, Q., F. Zhou, F. Ye, and S. J. Gao.** 2008. Genetic disruption of KSHV major latent nuclear antigen LANA enhances viral lytic transcriptional program. Virology **379:**234–244.
48. **Lim, C., Y. Gwack, S. Hwang, S. Kim, and J. Choe.** 2001. The transcriptional activity of cAMP response element-binding protein-binding protein is mod-

ulated by the latency associated nuclear antigen of Kaposi's sarcoma-associated herpesvirus. J. Biol. Chem. **276:**31016–31022.
49. **Lim, C., H. Sohn, Y. Gwack, and J. Choe.** 2000. Latency-associated nuclear antigen of Kaposi's sarcoma-associated herpesvirus (human herpesvirus-8) binds ATF4/CREB2 and inhibits its transcriptional activation activity. J. Gen. Virol. **81:**2645–2652.
50. **Lin, S. F., D. R. Robinson, J. Oh, J. U. Jung, P. A. Luciw, and H. J. Kung.** 2002. Identification of the bZIP and Rta homologues in the genome of rhesus monkey rhadinovirus. Virology **298:**181–188.
51. **Liu, J., H. J. Martin, G. Liao, and S. D. Hayward.** 2007. The Kaposi's sarcoma-associated herpesvirus LANA protein stabilizes and activates c-Myc. J. Virol. **81:**10451–10459.
52. **Lu, F., L. Day, S. J. Gao, and P. M. Lieberman.** 2006. Acetylation of the latency-associated nuclear antigen regulates repression of Kaposi's sarcoma-associated herpesvirus lytic transcription. J. Virol. **80:**5273–5282.
53. **Lu, F., L. Day, and P. M. Lieberman.** 2005. Kaposi's sarcoma-associated herpesvirus virion-induced transcription activation of the ORF50 immediate-early promoter. J. Virol. **79:**13180–13185.
54. **Mansfield, K. G., S. V. Westmoreland, C. D. DeBakker, S. Czajak, A. A. Lackner, and R. C. Desrosiers.** 1999. Experimental infection of rhesus and pig-tailed macaques with macaque rhadinoviruses. J. Virol. **73:**10320–10328.
55. **Mark, L., O. B. Spiller, M. Okroj, S. Chanas, J. A. Aitken, S. W. Wong, B. Damania, A. M. Blom, and D. J. Blackbourn.** 2007. Molecular characterization of the rhesus rhadinovirus (RRV) ORF4 gene and the RRV complement control protein it encodes. J. Virol. **81:**4166–4176.
56. **Miller, G., L. Heston, E. Grogan, L. Gradoville, M. Rigsby, R. Sun, D. Shedd, V. M. Kushnaryov, S. Grossberg, and Y. Chang.** 1997. Selective switch between latency and lytic replication of Kaposi's sarcoma herpesvirus and Epstein-Barr virus in dually infected body cavity lymphoma cells. J. Virol. **71:**314–324.
57. **Moorman, N. J., D. O. Willer, and S. H. Speck.** 2003. The gammaherpesvirus 68 latency-associated nuclear antigen homolog is critical for the establishment of splenic latency. J. Virol. **77:**10295–10303.
58. **O'Connor, C. M., B. Damania, and D. H. Kedes.** 2003. De novo infection with rhesus monkey rhadinovirus leads to the accumulation of multiple intranuclear capsid species during lytic replication but favors the release of genome-containing virions. J. Virol. **77:**13439–13447.
59. **O'Connor, C. M., and D. H. Kedes.** 2007. Rhesus monkey rhadinovirus: a model for the study of KSHV. Curr. Top. Microbiol. Immunol. **312:**43–69.
60. **Orzechowska, B. U., M. F. Powers, J. Sprague, H. Li, B. Yen, R. P. Searles, M. K. Axthelm, and S. W. Wong.** 2008. Rhesus macaque rhadinovirus-associated non-Hodgkin's lymphoma: animal model for KSHV-associated malignancies. Blood **112:**4227–4234.
61. **Pan, H. Y., Y. J. Zhang, X. P. Wang, J. H. Deng, F. C. Zhou, and S. J. Gao.** 2003. Identification of a novel cellular transcriptional repressor interacting with the latent nuclear antigen of Kaposi's sarcoma-associated herpesvirus. J. Virol. **77:**9758–9768.
62. **Pearce, M., S. Matsumura, and A. C. Wilson.** 2005. Transcripts encoding K-12, v-FLIP, v-cyclin, and the microRNA cluster of Kaposi's sarcoma-associated herpesvirus originate from a common promoter. J. Virol. **79:** 14457–14464.
63. **Pratt, C. L., R. D. Estep, and S. W. Wong.** 2005. Splicing of rhesus rhadinovirus R15 and ORF74 bicistronic transcripts during lytic infection and analysis of effects on production of vCD200 and vGPCR. J. Virol. **79:**3878–3882.
64. **Radkov, S. A., P. Kellam, and C. Boshoff.** 2000. The latent nuclear antigen of Kaposi sarcoma-associated herpesvirus targets the retinoblastoma-E2F pathway and with the oncogene Hras transforms primary rat cells. Nat. Med. **6:**1121–1127.
65. **Rainbow, L., G. M. Platt, G. R. Simpson, R. Sarid, S. J. Gao, H. Stoiber, C. S. Herrington, P. S. Moore, and T. F. Schulz.** 1997. The 222- to 234-kilodalton latent nuclear protein (LNA) of Kaposi's sarcoma-associated herpesvirus (human herpesvirus 8) is encoded by orf73 and is a component of the latency-associated nuclear antigen. J. Virol. **71:**5915–5921.
66. **Renne, R., C. Barry, D. Dittmer, N. Compitello, P. O. Brown, and D. Ganem.** 2001. Modulation of cellular and viral gene expression by the latency-associated nuclear antigen of Kaposi's sarcoma-associated herpesvirus. J. Virol. **75:**458–468.
67. **Renne, R., D. Blackbourn, D. Whitby, J. Levy, and D. Ganem.** 1998. Limited transmission of Kaposi's sarcoma-associated herpesvirus in cultured cells. J. Virol. **72:**5182–5188.
68. **Renne, R., D. Dittmer, D. Kedes, K. Schmidt, R. C. Desrosiers, P. A. Luciw, and D. Ganem.** 2004. Experimental transmission of Kaposi's sarcoma-associated herpesvirus (KSHV/HHV-8) to SIV-positive and SIV-negative rhesus macaques. J. Med. Primatol. **33:**1–9.
69. **Renne, R., M. Lagunoff, W. Zhong, and D. Ganem.** 1996. The size and conformation of Kaposi's sarcoma-associated herpesvirus (human herpesvirus 8) DNA in infected cells and virions. J. Virol. **70:**8151–8154.
70. **Renne, R., W. Zhong, B. Herndier, M. McGrath, N. Abbey, D. Kedes, and D. Ganem.** 1996. Lytic growth of Kaposi's sarcoma-associated herpesvirus (human herpesvirus 8) in culture. Nat. Med. **2:**342–346.
71. **Rice, P., I. Longden, and A. Bleasby.** 2000. EMBOSS: the European Molecular Biology Open Software Suite. Trends Genet. **16:**276–277.
72. **Sakurada, S., H. Katano, T. Sata, H. Ohkuni, T. Watanabe, and S. Mori.** 2001. Effective human herpesvirus 8 infection of human umbilical vein endothelial cells by cell-mediated transmission. J. Virol. **75:**7717–7722.
73. **Sarid, R., J. S. Wiezorek, P. S. Moore, and Y. Chang.** 1999. Characterization and cell cycle regulation of the major Kaposi's sarcoma-associated herpesvirus (human herpesvirus 8) latent genes and their promoter. J. Virol. **73:** 1438–1446.
74. **Schafer, A., X. Cai, J. P. Bilello, R. C. Desrosiers, and B. R. Cullen.** 2007. Cloning and analysis of microRNAs encoded by the primate gammaherpesvirus rhesus monkey rhadinovirus. Virology **364:**21–27.
75. **Schwam, D. R., R. L. Luciano, S. S. Mahajan, L. Wong, and A. C. Wilson.** 2000. Carboxy terminus of human herpesvirus 8 latency-associated nuclear antigen mediates dimerization, transcriptional repression, and targeting to nuclear bodies. J. Virol. **74:**8532–8540.
76. **Searles, R. P., E. P. Bergquam, M. K. Axthelm, and S. W. Wong.** 1999. Sequence and genomic analysis of a rhesus macaque rhadinovirus with similarity to Kaposi's sarcoma-associated herpesvirus/human herpesvirus 8. J. Virol. **73:**3040–3053.
77. **Shamay, M., A. Krithivas, J. Zhang, and S. D. Hayward.** 2006. Recruitment of the de novo DNA methyltransferase Dnmt3a by Kaposi's sarcoma-associated herpesvirus LANA. Proc. Natl. Acad. Sci. USA **103:**14554–14559.
78. **Soulier, J., L. Grollet, E. Oksenhendler, P. Cacoub, D. Cazals-Hatem, P. Babinet, M. F. d'Agay, J. P. Clauvel, M. Raphael, L. Degos, et al.** 1995. Kaposi's sarcoma-associated herpesvirus-like DNA sequences in multicentric Castleman's disease. Blood **86:**1276–1280.
79. **Staudt, M. R., and D. P. Dittmer.** 2006. Promoter switching allows simultaneous transcription of LANA and K14/vGPCR of Kaposi's sarcoma-associated herpesvirus. Virology **350:**192–205.
80. **Stedman, W., Z. Deng, F. Lu, and P. M. Lieberman.** 2004. ORC, MCM, and histone hyperacetylation at the Kaposi's sarcoma-associated herpesvirus latent replication origin. J. Virol. **78:**12566–12575.
81. **Storey, J. D., and R. Tibshirani.** 2003. Statistical significance for genomewide studies. Proc. Natl. Acad. Sci. USA **100:**9440–9445.
82. **Talbot, S. J., R. A. Weiss, P. Kellam, and C. Boshoff.** 1999. Transcriptional analysis of human herpesvirus-8 open reading frames 71, 72, 73, K14, and 74 in a primary effusion lymphoma cell line. Virology **257:**84–94.
83. **Verma, S. C., S. Borah, and E. S. Robertson.** 2004. Latency-associated nuclear antigen of Kaposi's sarcoma-associated herpesvirus up-regulates transcription of human telomerase reverse transcriptase promoter through interaction with transcription factor Sp1. J. Virol. **78:**10348–10359.
84. **Verma, S. C., K. Lan, and E. Robertson.** 2007. Structure and function of latency-associated nuclear antigen. Curr. Top. Microbiol. Immunol. **312:** 101–136.
85. **West, J., and B. Damania.** 2008. Upregulation of the TLR3 pathway by Kaposi's sarcoma-associated herpesvirus during primary infection. J. Virol. **82:**5440–5449.
86. **Wong, L. Y., G. A. Matchett, and A. C. Wilson.** 2004. Transcriptional activation by the Kaposi's sarcoma-associated herpesvirus latency-associated nuclear antigen is facilitated by an N-terminal chromatin-binding motif. J. Virol. **78:**10074–10085.
87. **Wong, L. Y., and A. C. Wilson.** 2005. Kaposi's sarcoma-associated herpesvirus latency-associated nuclear antigen induces a strong bend on binding to terminal repeat DNA. J. Virol. **79:**13829–13836.
88. **Wong, S. W., E. P. Bergquam, R. M. Swanson, F. W. Lee, S. M. Shiigi, N. A. Avery, J. W. Fanton, and M. K. Axthelm.** 1999. Induction of B-cell hyperplasia in simian immunodeficiency virus-infected rhesus macaques with the simian homologue of Kaposi's sarcoma-associated herpesvirus. J. Exp. Med. **190:**827–840.
89. **Ye, F. C., F. C. Zhou, S. M. Yoo, J. P. Xie, P. J. Browning, and S. J. Gao.** 2004. Disruption of Kaposi's sarcoma-associated herpesvirus latent nuclear antigen leads to abortive episome persistence. J. Virol. **78:**11121–11129.
90. **You, J., V. Srinivasan, G. V. Denis, W. J. Harrington, Jr., M. E. Ballestas, K. M. Kaye, and P. M. Howley.** 2006. Kaposi's sarcoma-associated herpesvirus latency-associated nuclear antigen interacts with bromodomain protein Brd4 on host mitotic chromosomes. J. Virol. **80:**8909–8919.